Optimization of marsh terracing as a wetland restoration technique: Mitigation of cohesive sediment erosion by waves associated with frontal passage

By

Joseph Edward French

Approved by:

Adam Skarke (Major Professor)
Jamie L. Dyer
Anna Linhoss
Alex Beebe
Renee M. Clary (Graduate Coordinator)
Rick Travis (Dean, College of Arts & Sciences)

A Thesis
Submitted to the Faculty of
Mississippi State University
in Partial Fulfillment of the Requirements
for the Degree of Master of Science
in Geology
in the Department of Geosciences

Mississippi State, Mississippi

May 2020

Name: Joseph Edward French

Date of Degree: May 1, 2020

Institution: Mississippi State University

Major Field: Geology

Major Professor: Adam Skarke

Title of Study: Optimization of marsh terracing as a wetland restoration technique: Mitigation of cohesive sediment erosion by waves associated with frontal passage

Pages in Study: 93

Candidate for Degree of Master of Science

Rates of marsh wetland loss in the northern Gulf of Mexico are the highest observed in North America. Marsh terraces have been implemented over the last 30 years to address this loss. Marsh Terraces reduce fetch and resulting wave energy which, reduces rates erosion of sediments in coastal wetlands. This thesis evaluated marsh terraces by extensive data collection that will assess the spatiotemporal relationships between wind patterns, wave parameters, and sediment strength in water bodies modified with marsh terraces. Data collected during two four-month deployments captured the passage of 40 cold front storms and the passage of Hurricane Barry. Results indicated that the mean threshold for erosion for marsh platform and terraces (0.194 N/m^2 and 0.500 N/m^2) were often exceeded during the passage of cold front storms. Orientation to reduce the influence of these storms was determined to be 270º/55º which is perpendicular to cold front associated winds.

ACKNOWLEDGEMENTS

This research was funded by the National Academies of Sciences, Engineering, and Medicine (grant # NAS2000008944). I am thankful for their funding of my graduate research assistantship to study marsh terraces as part of a wonderful research group. I also want to thank Ducks Unlimited Inc for their immense support to see this project to its finish. Thanks to Rockefeller Wildlife Refuge and the Louisiana Department of Wildlife and Fisheries for housing, materials, and boat support during our fieldwork. Thanks to the Miami Corporation for access to their properties for instrument deployment and sample collection.

A special thanks to Madelyn McFarland who always supported my research while deploying instruments and collecting data. Her expertise and knowledge of coastal Louisiana wetlands made navigation and general field work and absolute joy.

I am beyond grateful for my major advisor, Dr. Adam Skarke, who tirelessly supported me during my graduate studies. His high standard of academic excellence and devotion to students pushed myself to a much higher level than I thought I would achieve. For this I am greatly indebted to him as I feel my growth as a scientist is a direct result of his leadership.

I would like to thank my committee members Dr. Alex Beebe, Dr. Anna Linhoss, and Dr. Jamie Dyer for mentoring and guiding me during this experience. Their contributions to this work have made this an outstanding experience and instilled much confidence in myself to pursue a career in the geosciences.

Lastly, I would like to thank my wife Katrina, for her love and support during the past two years. She has made significant sacrifice to enable myself the time finish this master's thesis. And to my son Jack, I love you and I dedicate this to you.

TABLE OF CONTENTS

LIST OF TABLES

LIST OF FIGURES

CHAPTER I

PROJECT OVERVIEW

Coastal wetlands provide several ecological and physical services including the reduction of storm surge inundation from hurricanes, habitat for marine species including commercially important fisheries, and recreational areas (Costanza et al., 2008, Ruckleshaus et al., 2013). Coastal wetland loss rates in the northern Gulf of Mexico are the highest in the conterminous United States due to the combined effects of eustatic sea level rise, regional subsidence, and anthropogenic modification of local hydrological and sediment deposition regimes (Gosselink et al. 1998). Between 1956 and 2000 Louisiana lost 3950 km^2 of wetlands and the wetland loss rate was estimated to be 62 km^2 per year (Barras et al., 2003, Reed and Wilson 2004). The rapid conversion of wetlands to open water has resulted in a myriad of environmental engineering responses designed to restore coastal wetlands (Brasher 2015). These restoration efforts have focused on slowing wetland loss rates and, in some instances, accreting subaerial sediment to create new wetlands.

The goals of this thesis are to quantify the environmental conditions that drive erosive wetland loss, assess the capacity of marsh terraces to mitigate that loss, and prescribe design parameters that result in the maximum efficacy of terrace projects. Observational data collected at two wetland study sites in coastal Louisiana were used to address the following two hypotheses:

1) The primary source of erosive stress in the wetland study sites is wave energy created by the passage of cold front storms.
2) Marsh terraces are an effective means of mitigating wave induced erosive stress in the wetland study sites.

Specifically, this research used field observations to evaluate the capacity of marsh terraces to reduce the erosive potential of wind driven waves relative to the mechanical strength of soils composing the adjacent marsh platform as well as the terraces themselves. Wave conditions were measured with four acoustic Doppler current profiler (ADCP) instruments deployed at two marsh terrace sites for approximately four months each. These instruments recorded spectral wave height, wave period, wave direction, water level, and water temperature with a sampling frequency of one hour. During these deployments, a proximal sonic anemometer was also deployed on a three-meter mast in the center of each site. The anemometer measured wind direction and velocity with a sampling frequency of one minute. A series of representative submarine sediment samples were collected from five terrace and five marsh platform locations at each site. The resulting ADCP data were processed to determine the bed shear stress force imparted on the marsh platform and marsh terraces by observed wave conditions. Additionally, the sediment samples were analyzed in a laboratory to determine their shear strength (critical threshold for erosion) and therefore their mechanical resistance to the bed shear stress imparted by wave conditions. Finally, the anemometer data and coincident NOAA National Weather Service observations were used to establish the meteorological conditions (particularly wind directions and velocities) temporally coincident with wave conditions capable of eroding the marsh platform or terraces at each study site. Collectively these results indicate the environmental conditions responsible for a majority of erosive wetland loss in the study areas

and suggests terrace design parameters that are most important in mitigating the effects of such conditions.

CHAPTER II

LITERATURE REVIEW

GEOLOGIC SETTING

The present sedimentological and geomorphological properties of coastal Louisiana are largely a result of deltaic deposition by the broadly meandering Mississippi River over the past 7,500 years (Blum and Roberts, 2012) (Figure 2.1). Long term deltaic deposition of fine-grained fluvial sediments on a relatively low energy coast resulted in the development of extensive intertidal wetlands along the northern Gulf of Mexico. The geologic record indicates that these wetlands have generally kept pace with eustatic sea level rise since the last glacial maximum, migrating with the transgressive retreat of the shoreline (Blum and Roberts, 2012). However, modern coastal wetlands in Louisiana no longer appear to be adapting to relative sea level rise in the same manner. Rather, they are undergoing rapid loss with 1.2 million acres (4856 km^2) of coastal marsh being converted to open water between 1932 and 2011, and an additional 1.1 million acres (4452 km^2) expected to be submerged by 2060 (Couvillion et al., 2011). This broad scale change in coastal processes is attributable to the combined effects of accelerating eustatic sea level rise, regional subsidence, and recent anthropogenic modification of local hydrological and sediment deposition regimes (Gosselink et al. 1998).

Figure 2.1 Chenier and Mississippi River delta plain extent in coastal Louisiana and east Texas. The Mississippi River Delta extent (red) is fed by sediment supplied from the Mississippi River. The Chenier plain extent (yellow) is fed by various smaller tributaries that supply less sediment to build coastal wetlands.

The Chenier Plain of Louisiana is the western deltaic plain that extends from east Texas to Vermillion Bay, Louisiana. The Chenier Plain is underlain by the remnants of the Salé-Cypremont (> 4600 ybp) and Teche (3900-2800 ybp) deltaic lobes of the Mississippi River (Kolb and Lopik 1958). The switching of depositional deltaic lobes through the recent geologic past in the Chenier Plain region has created distinct depositional sequences that prograde into the Gulf of Mexico and exhibit a diagnostic sandy sequence (Hoyt, 1969). The surface stratigraphy of the interior portions of the Chenier Plain primarily consist of late Holocene muddy sediments (Owen, 2008). Coastal deposits in the Chenier Plain are primarily the result of longshore transport and wave reworking of deltaic deposits. Longshore transport is the primary source of coastal sediment input in the region because riverine sediment inputs into the Chenier plain are typically captured by large inland sinks such as the Calcasieu and Sabine lakes (Morton, 2017).

The Mississippi Deltaic Plain is the result of modern fluvial-deltaic distributary channels delivering sediment to the coastal region. The most current active sedimentation lobe of the Mississippi River was formed approximately 550 ybp (Morton, 2017). Currently, this deltaic region provides 80-90% of freshwater entering the Gulf of Mexico and 95% of sediment entering the northern Gulf of Mexico (Morton, 2017). Sediment transported by the Mississippi River historically fed wetlands and contributed to marsh wetlands ability to keep pace with sea level change throughout different periods of time (Day Jr., et al., 2007). Sediments that feed the active sedimentation lobe have resulted in primarily late Holocene sediments comprising most of the surficial framework of the Mississippi River Valley and Mississippi River Delta Plain (Owen, 2008).

Modern wetland loss in in coastal Louisiana is the result of the complex interaction of several natural and anthropogenic processes including accelerated eustatic sea level rise, subsidence, reduced sediment loads in the Mississippi river system, introduction of flood control structures, construction of industrial canals, elevated salinity resulting from alteration of the hydrological system, and tropical storms (Craig et al. 1979, Gosselink et al. 1998). This loss represents a significant threat to habitats, communities, and industry in the region (Yuill, et al., 2009). As marsh is converted into open water, its ability to serve as a buffer against storm waves and surges is degraded and important commercial and recreational fisheries are impacted by the loss of habitat critical to coastal species (Lovelace and Smee, 2018). Over the next 50 years, strong storms are predicted to erode approximately 4,500 km^2 of wetlands and produce storm surges that could cause an estimated 23 billion dollars of damage (Peyronnin, 2012). Given this forecast, both public and private coastal stakeholders are especially motivated to proactively seek solutions to slow or reverse wetland loss. Specifically, state government

agencies have taken a strong interest in understanding and addressing this problem, as outlined in the Louisiana Coastal Master Plan (LCPRA, 2012).

Current sea level and global climate trends indicate that sea level in the Gulf of Mexico (GOM) will continue to rise for the foreseeable future, with a total increase of 10-30 cm low estimate and 2.5 meters extreme estimate by the year 2100 (Sweet et al., 2017). Extensive land subsidence in concert with rising eustatic sea level will result in even higher rates of relative sea level rise in coastal Louisiana, further threatening wetland environments (Coleman and Roberts, 1989; Boesch et al., 1994). Modern hydraulic engineering measures designed to control flooding and maintain safe navigation in the lower Mississippi River have resulted in the accelerated transport of fluvial sediment offshore and in turn reduced sediment input into coastal wetland systems (Smith and Bentley, 2014). Restoration techniques focused on reducing wetland loss are an important tool for mitigating the potential hazards of rising sea level, subsidence, and sediment bypassing in coastal Louisiana wetlands. These approaches have largely focused on mitigating one of the direct causes of wetland loss or producing emergent wetland by modifying sediment transport processes so that deposition rates exceed rates are increased (Smith and Bentley, 2014).

MARSH TERRACING

Marsh terracing is a relatively new wetland restoration technique developed to mitigate wetland erosion by wind driven waves. It is based on the Shcleswick Holstein Method, which was originally developed in the Netherlands in the late 1800's and relied on the creation of drainage ditches in low lying intertidal areas to trap sediment and promote growth of new wetlands (Blum and Roberts, 2012). Modern marsh terraces on the US Gulf Coast are linear

segmented ridges constructed from mounded and compacted *in situ* sediment, which is primarily organic rich, fine-grained cohesive mixture of silt and clay (Turner and Streever, 2002). Marsh terraces are designed to create hydrodynamic conditions within wetlands that mitigate marsh erosion and promote emergent marsh growth and in turn promote the increase of marsh species population and diversity by providing a stable habitat (Brasher, 2015). Over 980 linear km of marsh terraces, which encompass a wide range of designs, have been constructed in coastal Texas and Louisiana since 1994 (Figure 2.2). The first known marsh terracing project was completed in 1994 under the authorization of the Coastal Wetlands Planning, Protection and Restoration act of 1990 (CWPPRA) (Trahan, 2017). The CWPPRA has provided 40 million dollars of grant funding annually to design and implement projects that focus on marsh restoration (Reed and Wilson 2004). Since the mid 1990's, numerous marsh terrace projects have been constructed between East Bay in Texas and the terminus of the Mississippi River in Louisiana with about 80 completed project sites to date (Brasher 2015).

As noted, marsh terraces are composed of submerged marsh sediments that have been dredged from borrow pits and deposited in adjacent linear berms that rise above water level (Turner and Streever, 2002) (Figure 2.4). Terraces are built to have surface platform elevations approximately 0.45 meters above mean sea level (MSL) (Underwood et al., 1991) and often newly created marsh terraces will be planted with *Spartina Alterniflora,* a species of common cord grass with root structure that can increase the structural stability of the terraces (Turner and Streever, 2002). Cordgrass plugs are systematically planted and spaced at regular intervals in the newly excavated sediments (Lindquist, 2008). Submerged aquatic vegetation (SAV) is also planted in some cases, with the expectation that the vegetation will be able to reduce sediment

loading in the water column by slowing water flow velocity and promoting the settling of suspended sediments (Underwood et al., 1991). Terraces are often arranged in geometric patterns across open water areas within marshes to maximize the disruption of large areas of potential fetch (Thayer et al., 2005). The dimensions of terraces vary significantly across project sites, but terraces are usually built in a consistent manner within an individual project site. The most common terrace shapes are chevron pattern, followed by linear and rectangular designs. Terraced projects can also be quite variable as some of the designs seem experimental or *ad hoc* in nature. Given the wider range of implemented terrace designs, there is a need to quantitatively assess, the design parameters that most contribute to the success of a terracing project, in order to optimize future terrace implementation.

Research focused on the efficacy of marsh terrace projects has been conducted at several project sites. Many of these studies have focused on ecological aspects of the terraces, such as their effect on fishery habitats, waterfowl densities, and nektonic organism populations (Rozas and Minello, 2001; La Peyre et al., 2007; O'Connell and Nyman, 2010; Lovelace and Smee, 2018;). However, very little research has focused on the longevity of marsh terraces or their impact on physical process that control sediment erosion as well as accretion which ultimately affect coastal wetland creation or loss.

Initial results of remote sensing analysis indicate that some marsh terrace projects have exhibited net sediment accretion after construction; however, definitive causative mechanisms for this remain speculative (Osorio et al., 2020). Despite widespread implementation and encouraging preliminary results, the success of specific marsh terrace projects and efficacy of marsh terracing as a wetland restoration technique has yet to be fully and thoroughly investigated (Brasher, 2015). Initial observations indicate that a wide range of complex

interrelated environmental factors determine the success and ultimate longevity of terrace projects. Quantifying those factors and understanding their relationships critically informs future marsh terrace development and implementation, particularly optimization of terrace project design for efficiency and efficacy.

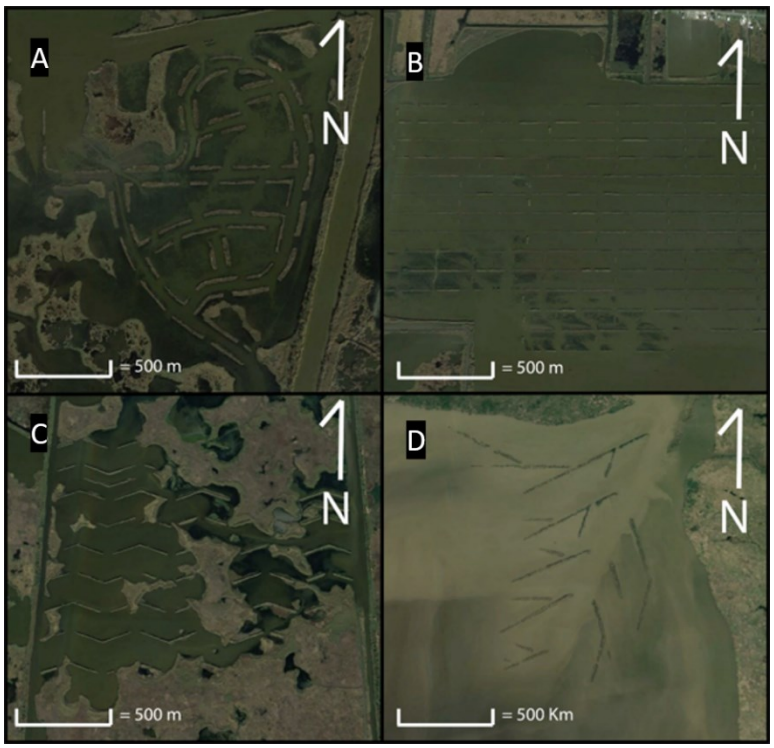

Figure 2.2 Four different marsh terraced fields in southern Louisiana exhibiting variation in shape and orientation. A. Marsh terraces in an *Ad Hoc* style. C. Marsh terraces in a semi-box like pattern. C. Marsh terraces in a chevron pattern. D. Marsh terraces in a semi-dendritic pattern.

A primary design consideration of marsh terraces is disruption of wind-wave fetch and creation of additional marsh edge (Rozas and Minello, 2001). Fetch is the distance over which wind can exert shear stress on the surface of a body of water to create waves (Figure 2.3). One quantitative measure of the restoration efficacy of marsh terracing is the degree to

which terraces are able to reduce fetch and therefore incident wave energy (parameterized as wave generated bed shear stress) on the marsh platform and on the terraces themselves (Rozas and Minello, 2001; Steyer et al., 2003; Underwood et al., 1991) (Figure 2.4 & 2.5). An additional measure of restoration efficacy of marsh terracing is the degree to which they reduce suspended sediment concentrations in the water column through the prevention of erosion or the promotion of deposition (Steyer et al., 1993, Turner and Streever, 2002).

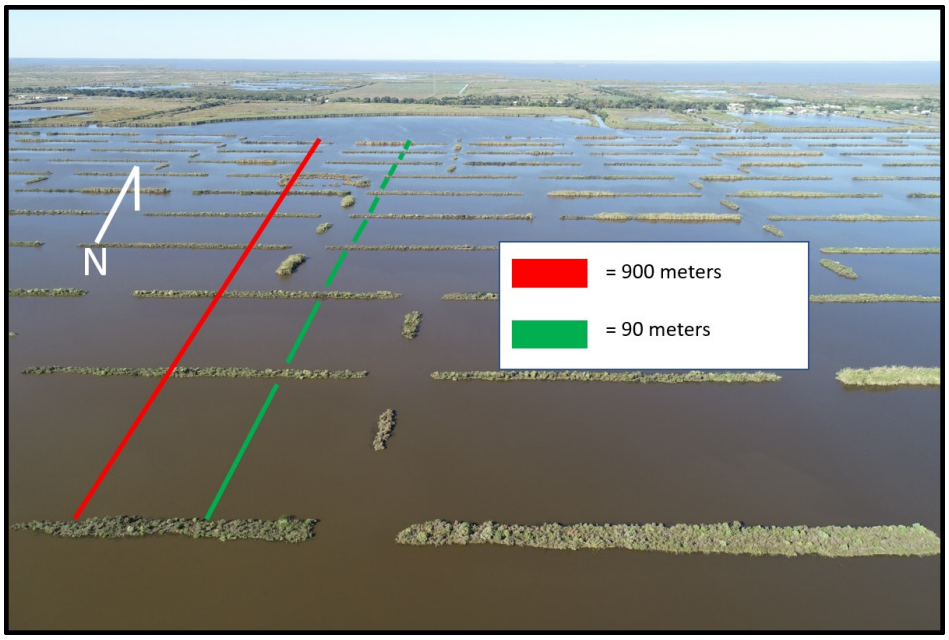

Figure 2.3 Conceptual diagram of marsh terraces segmenting fetch. Assuming a north wind blowing the terraces will segment 900 meters of fetch into 90-meter segments.

A persistent question related to marsh terrace design is the optimal orientation(s), spacing, and shape of terrace structures to minimize effective fetch and resultant wave erosion. Existing terrace projects have pursued a range of design approaches and it is not yet clear which design elements have resulted in the greatest success regarding mitigation of wave erosion and promotion of new marsh growth (Lindquist, 2008). Quantifying the orientation, spacing, and

shapes of marsh terraces relative to wind fields from different atmospheric processes, such as cold fronts and daily wind patterns, may inform optimal designs for future terraces to best counter wind conditions that produce the most erosive waves.

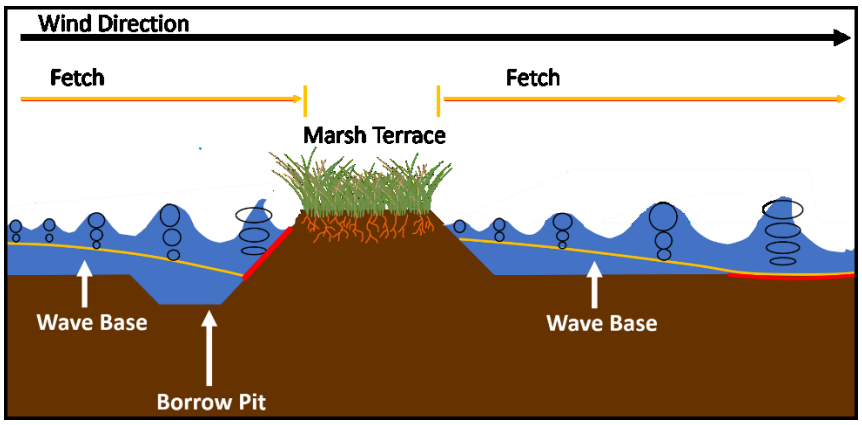

Figure 2.4 Diagram of a single terrace breaking fetch and wave energy. Approaching waves on left side of terrace are limited in size due to terrace. The disruption of fetch results in smaller waves on the right side of the terrace having to re-generate with distance and duration of wind.

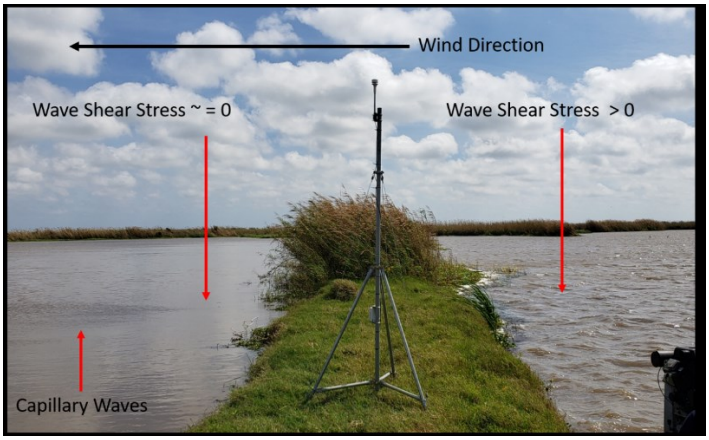

Figure 2.5 Example of a single terrace breaking wind fetch thus inhibiting waves with significant height to propagate across the water body. At some distance past the terrace capillary waves are starting to generate and will increase in height as they move away from terrace.

COLD FRONT PASSAGES

Cold front storms are associated with the boundaries between heterogenous air masses in which a colder dry air mass is pushing a warm moist air mass (Nese and Grencki, 2006). These storms move across the northern Gulf of Mexico region with a frequency of 20-30/yr, primarily during the fall and winter (October- April) (Roberts et al., 2015). Open water bodies that exist in the wetlands of the Chenier and Mississippi River Delta Plains are at risk of losing sediments due to cold front passage. Specifically, cold fronts commonly generate wind fields sufficient to create waves that erode, suspend, and transport sediment in coastal wetlands. The influences frontal passages have on local areas largely depend on the type of frontal passage (cold, warm, stationary). Cold front passages which are the most common weather system in the northern Gulf of Mexico region (Guo and Li, 2020). The leading edges of these storms bring significant wind velocity, precipitation, temperature changes, and reduction in water depth.

Differences the temperature and water content between advancing cold dry air masses and retreating warm moist air masses generate the storms observed during frontal passage. Sources for these two air masses differ spatially as the advancing cold dry air masses are sourced from polar artic regions (maritime Polar, mP) (Henry 1979). Warm moist air masses are sourced locally from the Gulf of Mexico region (maritime tropical mT) (Ahrens and Henson, 2012). The exact location of the source of cold air masses will determine the orientation in which cold fronts will pass through the northern Gulf of Mexico area but, the effect is still the same as large scale intense storms that have the capability to generate erosive waves will occur.

In the case of coastal wetlands in the northern Gulf of Mexico, water level set-up against the east-west oriented shoreline by strong southerly winds that preceded a cold-from passage, deepens water in coastal wetlands enabling the generation of larger waves (Huang and Li, 2020;

Li et al., 2010; Roberts et al., 2015) (Figure 2.6). Field observations have shown that the water level in marshes can rise by up to 0.95 meters during strong seasonal storms (Walker and Hammack, 2000) due to set-up and storm associated reduction in barometric pressure, which has been demonstrated to yield 0.1 meter of water level rise for every 10 mbar of pressure drop (Trosclair, 1995). Subsequent flushing of those wetlands by strong northerly winds flowing a cold front pushes water laden with newly suspended sediment out of the wetland into the Gulf of Mexico, where it can be sequestered (Feng and Li, 2010). Sediments transported offshore beyond the fair weather wave base may be sequestered from the wetlands for extended periods of time and sediments transported beyond the storm wave base will likely be permanently removed from the coastal wetland sediment budget (Turner et al., 2006; Guo and Li, 2020). The frequency of cold fronts and their potential to redistribute sediment stared wetlands presents serious challenges to restoration efforts in the northern Gulf of Mexico (Guo and Li, 2020).

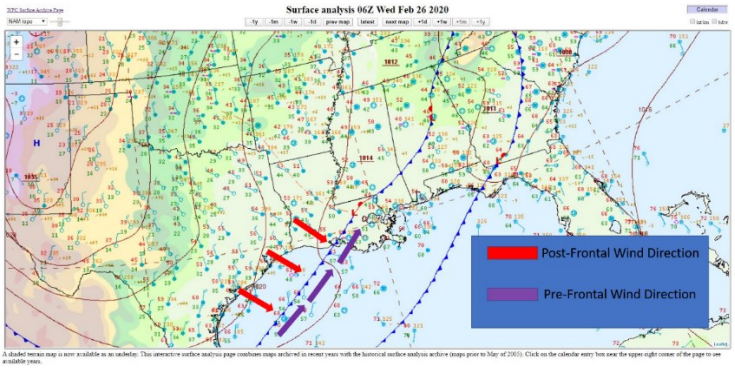

Figure 2.6 Cold front passage on Feb 26th, 2020. Conceptual arrows represent general wind direction at the surface during passage of storm. Purple arrows represent winds blowing out of the south as the storm approaches. Red arrows indicate the post frontal winds that are driving the cold dry air mass through the area. Surface analysis map generated from NOAA Weather Prediction Center archive of 3-hour interval surface maps.

HYDRODYNAMICS

INTRODUCTION

Marsh wetland environments are characterized by complex hydrodynamic and sediment transport processes that are occurring at the interface between marine and terrestrial environments. Because the Gulf of Mexico is microtidal, tidal current induced circulation in coastal wetlands is generally secondary to wave energy in terms of capacity to erode sediment. Moreover, the two wetland study sites utilized in this research are partially isolated from tidal exchange by anthropogenic modification of the local hydrology further reducing the impact of tidal circulation on sediment erosion. It should be noted that this is a typical condition for marsh terrace sites in coastal Louisiana. Accordingly, sediment erosion by wind driven wave processes is the primary hydrodynamic focus of this research.

GENERATION OF WAVES

Wind waves, at the scale considered in this thesis, are generated by a balance between the disturbing force of wind blowing over water (shear stress) and the restoring force of gravity (Fagherazzi and Wiberg, 2009). The growth of waves is a function of the velocity and direction of the generating wind as well as the uninterrupted distance of water over which that wind blows, which is known as fetch (Smith, 1991). Waves are characterized by a series of well-defined physical parameters, which includes height, wavelength, period, and speed (celerity). As waves propagate across the surface of a body of water, they generate orbital motion within the water column beneath the surface (Garrison and Ellis, 2018) that exponentially decays in magnitude downward to a depth that is equal to one half the wavelength. This depth is known as the depth of closure or wave base (Figure 2.4). When total water depth is less than the depth of closure wave orbital motion is incident with the bed and moves parallel to it, which exerts a frictional

force (bed shear stress) on bottom sediments (Myrhaug, 2017). Bed shear stress is a function of the velocity of wave orbital motion and the frictional forces created by seafloor roughness features including grain diameter, bedform height, and suspended sediment concentration. Wave orbital velocity is a function of wave height, wave period, and water depth (Dean and Dalrymple, 1992). Wave orbital velocities increase with increasing wave height and period but, decrease with increasing water depth (Wiberg and Sherwood, 2008). Due to the complexity of directly measuring frictional forces created by seafloor roughness in marsh environments, they are typically parameterized based upon modeled empirical relationships with the properties of the surface waves that generate them (Whitehouse et al., 2000). When wave generated bed shear stress exceeds the shear strength of bed sediments, erosion occurs (Fagherazzi and Wiberg, 2009).

Given the relationship described above the capacity for a wave to erode marsh sediment is a function of water depth, and wave parameters (wavelength, height, period), which are causally related to fetch. Simply stated, increasing the fetch in a marsh environment will increase wave size and thus the potential for wave erosion. This relationship is described in the following expression (Smith, 1991):

$$H = 0.0016 g^{-0.5} X^{0.5} U, \tag{2.1}$$

Where, H is the significant wave height, X is fetch, g is gravitational acceleration, and U is the time averaged velocity of windspeed for a sustained duration.

WAVES ORBITAL SHEAR STRESS

The shear stress imparted on the bed by waves orbital motion (τ_{0_w}) is expressed as (Soulsby et al., 1997):

$$\tau_{0_w} = \frac{1}{2}\rho f_w u_w^2 \tag{2.2}$$

Where ρ is the density of water and (u_w) is the significant wave orbital velocity at the bed expressed through linear wave theory as (Soulsby et al., 1997):

$$u_w = \frac{\pi H_s}{T \sinh(kh)} \tag{2.3}$$

where h is the localized water depth, H_s is the significant wave height (the mean of the highest one third of observed waves), T is the wave period, k is the wave number ($2\pi/L$), and L is the wavelength. The value f_w in equation 2.2 is the wave friction factor empirically determined for hydrodynamically smooth flow conditions over cohesive sediments as (Whitehouse et al., 2000):

$$f_w = BR_w^{-N} \tag{2.4}$$

where R_w is the wave Reynolds number, defined as:

$$R_w = \frac{u_w A}{v} \tag{2.5}$$

and:

$$B = 2, \qquad N = 0.5 \qquad for\ \ R_w \leq 5\ x\ 10^5$$
$$B = 0.0521, \qquad N = 0.187 \qquad for\ \ R_w > 5\ x\ 10^5 \tag{2.6}$$

The term v is the kinematic viscosity of water and the term $A = d_w/2$ where d_w is the significant wave orbital diameter at the bed expressed through linear wave theory as (Soulsby et al., 1997):

$$d_w = \frac{H_s}{\sinh(kh)} \tag{2.7}$$

The necessary environmental variables $h, H_s, T, L, \rho\ and\ \ v$ are typically measured for a giving study area with deployed instrumentation. The value for maximum wave shear stress τ_{0_w} (N/m^2) calculated with equation 2.2 can be directly evaluated relative to measured sediment shear strength which has the same dimensional units (N/m^2) to quantify the potential for bed erosion. Finally, instrumental observations of the time series of relative suspended sediment concentration as a function of water depth will indicate the amount of mobilized sediment in the marsh and timing of sediment transport events as they relate to wind, wave, and water level conditions.

SEDIMENT COHESIVE STRENGTH

INTRODUCTION TO COHESIVE SEDIMENT

Cohesive sediment is composed of clay and silt sized particles mixed with organic matter (Grabowski et al., 2011). Sediment particles are bound together by physiochemical surface forces and pore space is occupied by water and, in some cases, gas arising from the breakdown of organic material (e.g. methane and hydrogen sulfide) (Gerbert et al., 2006, Grabowski, 2011).

The critical threshold of erosion (τ_{cr}) for a sediment is the stress necessary to overcome the mechanical strength of a cohesive sediment and mobilize particles. This section will examine a variety of physical, geochemical, and biological properties that influence the mechanical strength and resultant critical threshold of erosion for cohesive sediments.

PHYSICAL FACTORS

The primary physical factors that determine the erodibility of cohesive sediments are mean particle size, size distribution, bulk density, water content, and temperature (Grabowski, 2011). Sand and coarser sized p (>62.5 μm) behave in intuitive ways under the influence of moving water, namely they exhibit a positive correlation between particle size and the hydrodynamic force necessary to erode it. However, find grained sediment (i.e. silt and clay) interparticle attractive forces have an increasing effect on the behavior of sediment. Behavior of these fine-grained sediment under hydrodynamic forcing is the result of organic coatings and adhesion of extra polymeric substances (EPS) that bind the grains together (Johnson et al., 1994; Lick et al., 2004). As the size of grains decreases, bulk density increases and the influence of other forces such as organic bonding and ionic bonding exert much more control of the erodibility of the sediment (Grawboski et al., 2011). A higher bulk density with smaller particle sizes drastically increases the threshold for erosion (Roberts et al., 1998).

The distribution of particle size can also affect the threshold for cohesive sediment erosion. It was found that clay content directly influences the threshold for erosion (Mitchener and Torfs, 1996; Panagiotopoulos et al., 1997; Grabowski et al., 2010). Once clay content is above 4-10% the framework of the sediment is cohesive (Grawboski, 2011). To demonstrate the effect of clay content on erosional rates work from (Houwing, 1999) showed that when clay content of sediment increased from 4-35% the erosional rates decreased by two orders of magnitude.

An additional physical factor that determines the threshold for erosion in a sediment is water content. Water can fill pore space in sediments, which can decrease the overall wet bulk density. (Jepsen et al., 1997; Lick and McNeil, 2001) indicate that erosional rates could be up to 100 times lower in dense beds with little pore space compared to less dense beds. Empirical relationships have been developed for water content values to predict the behavior of cohesive sediments (Amos et al. 2004).

GEOCHEMICAL FACTORS

The geochemical properties of sediments control the way in which inter particle attraction affects sediment strength. These geochemical properties can be broken into clay mineralogy, water geochemistry, pH, metal content, and organic content (Grabowski, 2011).

Clay mineralogy is a major geochemical property in cohesive sediment strength. Clay behavior is dependent upon clay particle sizes as particle size determines sediment properties such as plasticity, cation exchange capacity, water absorption, saline absorption rations (Brady and Weil 2005; Grim, 1962; Kandiah, 1974; Morgan, 2005; Partheniades, 2007). Previous research has divided clays into three major groups based on grain size. Clay type is classified by mean grain size as these categories will determine the behaviors of clays contributions to cohesive sediment strengths.

Clay surface inter particle attraction exerts greater influence than forces from gravity and decreasing grain size amplifies this affect (Harraz, 2014). The three primary clays groups are kaolinite, illite, and montmorillonite (Grabowski et al., 2011). Clays are primarily categorized by their mean grain size as the distribution of grain sizes will significantly influence the observed physical properties of cohesive sediment. Kaolinite is the largest grain size category of clay minerals. The large particle size results in sediments with low plasticity, low water absorption rates, and an overall low erodibility in sediments (Grabowski et al., 2011). Illite clays are described as having medium sized grains that result in increased plasticity which increases observed shear strengths.

Montmorillonite clay contains the smallest grain sizes that exhibit the strongest inter particle attraction which includes a high degree of plasticity resulting high shear stresses needed to entrain particles.

Water geochemistry is a major factor influencing the behavior of cohesive sediments as the dissolved ionic load (salinity) of water can influence clay behavior. Dissolved ions such as Na^{+}, Ca^{2+}, and Mg^{2+} can influence the amount of water absorbed by a sediment thus directly influencing the strength of cohesive sediment (Grabowski, 2011). Soils science has been particularly concerned with the sodium absorption rates (SAR the ratio of Na^{+} to Ca^{2+} concentrations in sediment) of soils as SAR> (13-15) is an indicator of clays that can expand with ease and indicate moments of high erodibility (Rowell, 1994; Brady and Weil, 2002). A study from (Kandiah, 1974) revealed that beds composed of pure montmorillonite had lower threshold for erosion values than kaolinite. But, when exposed to softer water the montmorillonite was determined to be more resistant than the kaolinite. Ultimately, water parameters such as ion load, and pH determine how clays behave and site-specific determinations of water geochemistry should be made for an accurate assessment of environmental conditions that may affect sediment strength.

Porewater pH is another property that influences the behavior of cohesive sediments. High pH will increase erodibility as the decrease in available H+ ions will result in the thickening of the double layer resulting in larger repulsive forces in the sediment (Wintwerp and Kesteren, 2004). Further research is still needed in this area as initial work as shown that the effects of pH may be highly dependent upon salinity levels of water.

Organic content from benthic organisms and decaying plants is another factor that influences the strength of cohesive sediments. Laboratory studies have shown that when dissolved organic matter (DOM) is added to kaolinite beds the stability is increased. The addition of DOM was found to lower the bulk density but, the threshold for erosion was increased by a factor 2-3 (Ravisangar et

al., 2005). Field observations also support the ability of organic matter to increase the threshold of erosion. In lacustrine settings, an increase of organic matter from 8-25% resulted in a 5-fold increase in sediment strength (Rigettie and Lucarelli, 2007). It was estimated though that the effect of organic material is maximal at 12-14%.

BIOLOGICAL FACTORS

Biological processes play a role in all sediment processes, to some degree, whether it be the influence of bacteria or larger organism at the macroscopic level such as invertebrates (Grabowski, 2011). Marine organisms, especially the benthic variety, can alter the sediment surface in such a way that alters cohesive and non-cohesive sediments alike. The impacts made by these organisms is generally described as bioturbation, bio stabilization, and bio destabilization (Black et al., 2002).

Bioturbation is the disturbance of sedimentary deposits by organisms, which commonly alter the sediment characteristics such as compaction, sorting, and structure (Meysman et al., 2006). Bio stabilization and bio destabilization can enhance or diminish sediment strength (Grabowski, 2011). Organisms can destabilize sediment through burrowing and stabilize sediments via biofilms that increase sediment strength or root systems, which establishing a network to further increase strength of sediments. Movement of organisms on the sediment surface and the process in which they feed and egest can influence sediment strengths (Grabowski, 2011). For example, it was found that the densities of Manila clams loosen sediments as their vertical movement increase the erodibility of the sediments (Sgro et al., 2005). Conversely, these organisms can contribute to the strength of sediment and can also increase sedimentation rates by capturing particles in the water column by depositing excrement onto the marine bed (Graf and Rosenburg, 1997; Wildish and Kristmanson, 1997). The last major

consideration of biologic impacts of cohesive sediment relationships is the network systems of roots, and extra polymeric substances (EPS). Strong fibrous root systems can absorb some amounts of tensile stress placed onto the bed (Simon et al., 2006). Larger root systems that spread throughout cohesive have much more potential to absorb even greater amounts of stress. EPS secreted from benthic organisms often bind to surface sediment resulting in an increase sediment shear strength. EPS is secreted from a variety organism from unicellular bacteria to many fish species (Wotton 2005).

CHAPTER III

METHODS

STUDY AREAS

This study focused on marsh terrace sites within the Chenier Plain in coastal Louisiana. This region extends laterally from Vermillion Bay in south-central Louisiana to East Bay, which is in southeastern Texas (Holmes et al., 2009). This study used two terraced sites for the collection of field data (Figure 3.1). Both sites have environmental and terrace characteristics that differ substantially, making them valuable for comparative study (Table 3.1 and Figure 3.1). The design of marsh terraces constructed in both study sites are different from each other and representative of the most commonly implemented terrace shapes on the Gulf Coast i.e., (Chevron and Rectangular). They are relatively close to each other (9 km) lying in the chenier plain which allows for the assumption that the same atmospheric forces and geological context that affect one will affect the other.

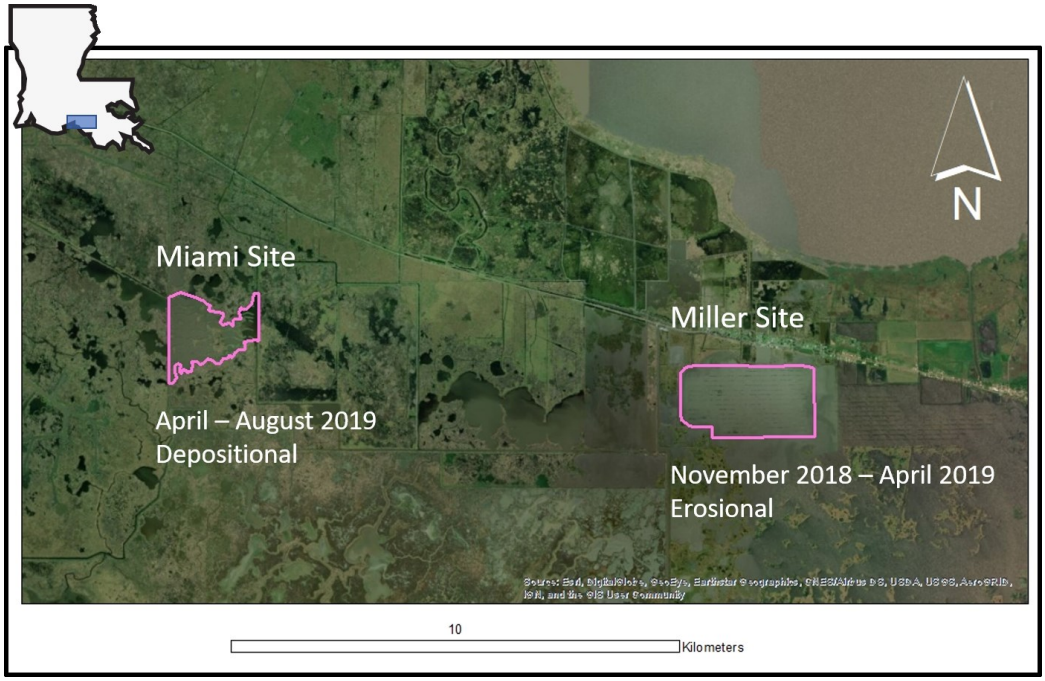

Figure 3.1 Map showing proximity of both terraced sites to each other (roughly 9 km of distance between the two sites).

Table 3.1 Marsh terrace physical characteristics at each study site

Variable	Miller property	Miami property
Individual Terrace Size (meters)	145x10 (E-W)	80x10 (Linear)
	35x10 (N-S)	300x10 (Chevron)
Terrace Shape	Linear North and South	North/South Chevron with 150^{o} Angle
Pond Area (km^2)	5.5	1.42
Deployment Dates	November 2018- April 2019	April 2019- September 2019

Water salinity levels are a key indicator of the marsh type and marsh community present (Penfound and Hathway 1938; Chabrack, 1970). The Coastwide Referencing

Management System uses multiple reference points throughout the Mississippi River Delta to record water quality conditions throughout the area (Steyer et al., 2003). Data from this system as accessed via the CRMS website was be utilized to determine salinity regimes present in the study area (CRMS, 2020). The Miller property was found to be a freshwater marsh with an average salinity of 0.96 ppt (a salinity of 35 is marine).

WAVES

Four Nortek 1000 Signature series acoustic Doppler profilers (ADCP) were deployed on upward looking frames to profile the water surface (Figure 3.2 and 3.3). The acoustic instruments recorded environmental and wave conditions for the full duration of the deployment with a sampling frequency of one hour. Recorded data included wave height, wave period, wave direction, water level, water temperature, and water column acoustic backscatter intensity, which can serve as a proxy for relative suspended sediment concentration. ADCP instruments were mounted in an upward looking orientation on frames that were deployed on the bottom of the marsh terrace study sites. The instruments measure wave parameters using five acoustic beams that record water surface elevation and water velocity in 2-cm bins between the water surface and a point approximately 10 cm above the instrument. Wave observations were made at a frequency of 8 Hz in order to capture the fundamental properties of individual propagating wave forms and wave orbital motion.

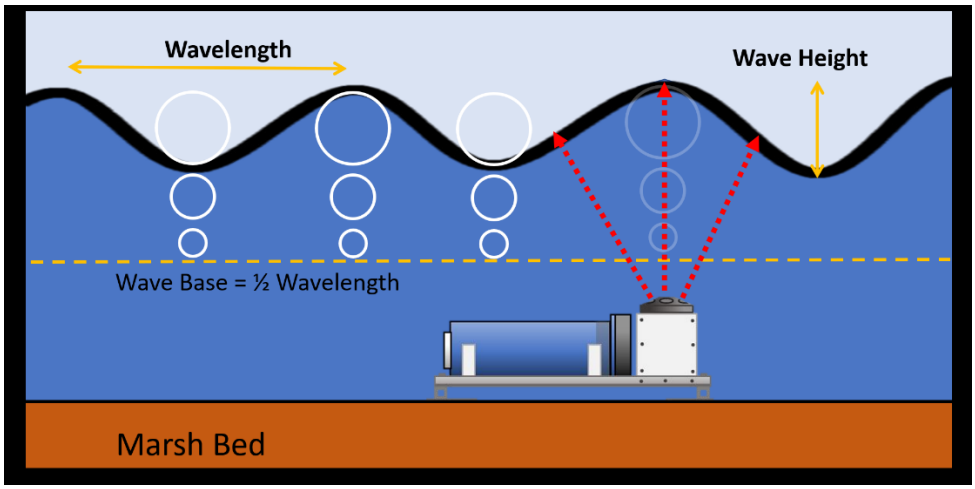

Figure 3.2 Conceptual diagram of an ADCP instrument mounted on deployment frame. Instrument is looking up at water surface profiling passing waves.

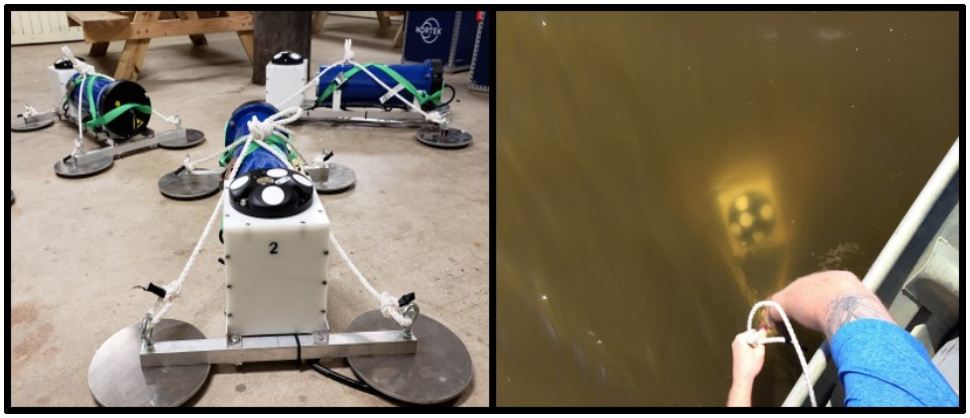

Figure 3.3 Nortek Signature 1000 ADCP Instruments were deployed to collect hydrodynamic data. ADCP instrument on frame (left) and instrument being lowered onto marsh bed (right).

At the study area, wave instruments were positioned to capture the range of conditions within the terraced area as well as boundary conditions outside the terraced area. This allowed for comparison of the relative influence of the terrace on wave conditions and was most appropriate for validating hydrodynamic numerical models of the terrace site being developed

by collaborators. The instruments were programmed to continuously record wave data at 8 Hz during 17-minute-long sampling "bursts" that occurred once an hour. These data were used to quantify the scope and magnitude of the wave conditions at the study site and evaluate the periods when wind conditions were fast enough to create waves with enough energy to erode the marsh platform and terraces.

Recovered data were imported into MATLAB to calculate orbital shear stress. Parameters recorded from ADCP instruments such as: wave period, wave height, wave direction, and water depth were processed by MATLAB. Developed code from Sherwood (1994) was used to calculate wave orbital shear stress using linear wave theory (Soulsby, 1997). The output from the code was time series observations of wave orbital shear stress in N/m^2.

SEDIMENT

The critical shear strength for sediments from marsh terraces and the surrounding marsh platform was determined through analysis of the bulk density of sediments. Bulk density is a property that can offer insight about a variety of properties such as water content and grain size distribution that can be used to calculate sediment strength over a large area (Grabowski et al., 2011). Bulk density results are used in latter portions of this study to calculate the erodibility of marsh platform and terrace sediments.

BULK DENSITY DETERMINATION

The bulk density of sediments was determined following established methods set forth by the United States Department of Agriculture's Soil Quality Test Kit Guide (USDA, 2001). Bulk density was measured for sediment sampled from the top 3 inches of the surficial sediments of

marsh terraces and surrounding marsh platform. Cohesive sediment was sampled from 5 locations of marsh terrace and 5 more samples from marsh platform sediments for a total of 10 samples at each study area.

RETRIEVAL OF SEDIMENT

Sediments samples were retrieved by extracting fully saturated sediments from the marsh platform and marsh terraces (Figure 3.4). Enough material was collected to conduct bulk density analysis on five replicates of each sample. Retrieved sediments were labeled, placed into sealed plastic sample bags, and immediately put on ice to preserve water content for wet bulk density testing.

Figure 3.4 Sediment excavated from natural marsh platform during field deployment. Fully saturated sediments were retrieved to test for wet bulk density. Samples taken at depths approximately 10-20 cm.

BULK DENSITY CALCULATION

Wet bulk density was determined by weighing sub samples of a known volume to calculate the density of the fully saturated sediment. Sub samples were taken with a 15 cm^3 measuring scoop and then weighed on a Denver Instrument S-2002 precision scale with accuracy to 0.01 gram. Prior to sub sampling each sample was mixed thoroughly in the sample bag by kneading until all the sediments in the sample are thoroughly mixed as indicated by USDA (2001). Five sub samples were taken from each sample and the corresponding weights were recorded. The following equations are used to determine the wet bulk density and other related variables once the dry weight of sediment has been determined:

$$Wet\ bulk\ density\ = \frac{Weight\ of\ Saturated\ Soil\ (g)}{Volume\ of\ Scoop\ (cm^3)} \tag{3.1}$$

CRITICAL SHEAR FROM BULK DENSITY

Estimations of the shear strength (τ_s) of each sediment sub sample were made from bulk density observations with the empirically relationship established by Mehta (1988):

$$\tau_{cr} = \zeta(Q_b - 1) \tag{3.2}$$

Where, τ_s is shear strength in N/m^2, Q_b is the wet bed bulk density in g/cm^3, and ζ =1 dimensionless coefficient for cohesive sediment.

METEROLOGICAL PHENOMENON

FRONTAL AND TROPICAL STORM PASSAGES

A consideration of the duration and frequency of erosional events that occur in coastal Louisiana has led to the hypothesis that the primary source of erosive stress in the wetland study sites is wave energy created by the passage of cold front storms. To evaluate this hypothesis, a multiyear record of surface analysis maps from the National Ocean Atmospheric Association (NOAA) was used to observe passage of frontal systems. Concurrently, a deployed anemometer was deployed to describe general patterns of wind direction, magnitude, and duration associated with cold fronts in coastal Louisiana. Specifically, surface analysis charts generated by the National Ocean Atmospheric Association (NOAA) Weather Prediction Center (WPC) were reviewed to determine when cold front events occurred at the study sites. The charts describe atmospheric conditions with a frequency interval of three (3) hours, which allows for relatively precise timing of when cold fronts pass over the study sites (Fig 3.5). Cold front timing was further refined by analysis of associated rapid wind shifts observed in anemometer data collected at each study site. The time series of surface winds and determined times of cold front passage were directly compared with time series of wave conditions and suspended sediment concentration at the study sites to determine if there is a temporal correlation between cold front passage and periods of elevated wave erosion.

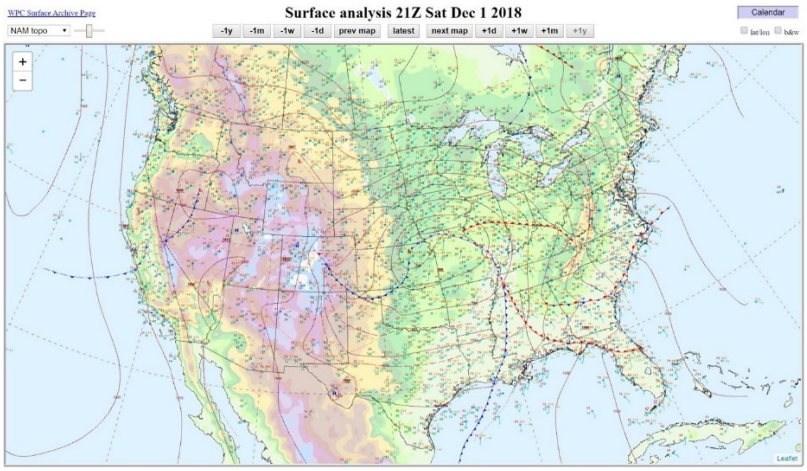

Figure 3.5 NOAA surface analysis map for the United States. A cold front air mass is indicated by the blue line over the state of Louisiana. Outward blue teeth on line indicate direction of the air masses movement.

ANEMOMETER DATA

A field anemometer was deployed to gather local time series data for wind direction and velocity at one-minute intervals (Figure 3.6). The device deployed was the HOBO H21 MicroStation which records at specified intervals while recording wind direction in degrees and wind velocity in meters per second. The sensor used was the Onset S-WCG-M003 ultrasonic wind sensor. At the time of deployment, the anemometer was oriented relative to north by using a sighting arm in order to reference collected data. This sensor recorded speeds (min 0.4 m/s and max 41 m/s) at one-minute intervals yielding a high degree of temporal resolution.

Figure 3.6 Sonic anemometer set up onto marsh terrace. Instrument is aligned to look north to give spatial reference for all recorded data.

CHAPTER IV

MILLER DEPLOYMENT

INTRODUCTION

The Miller property is located in the Chenier Plain of coastal Louisiana near Pecan Island (29.646178, -92.454523). The property lies just south of highway 82, just to the south of White Lake, and about 50 km east of Grand Chenier, Louisiana. From November 1st, 2018 to April 9th, 2019 (159 Days) four ADCP instruments and an anemometer were deployed to capture meteorological and hydrodynamic conditions at this site. Additionally, sediment samples were subsequently collected on February 2, 2019 to use in the calculation of terrace and marsh palatiform bulk density.

The area of the Miller property is approximately 2.75 km^2 with the marsh platform (natural marsh wetlands) immediately surrounding the north and west boundaries. The southern boundary is exposed to open water fetch of approximately 1.25 km. To the east another major set of terraces exist that that have a similar configuration. In between the two fields exist an area of open water with a fetch of 2.5 km in the northern to southern directions and 0.5 km in the eastern to western directions (Figure 4.1).

The terraces at the Miller property are linear and arranged in a semi-enclosed rectangular pattern (Figure 4.1). The terraces can be grouped into two major categories based on azimuthal orientation. The first group are oriented due east-west at about 89°. These terraces are approximately 150 meters long; although, their length can vary due to the amount of erosion

each terrace has been subject to. Terrace width also varies slightly across the study site, but the mean width is about 10 meters across. The second group of marsh terraces are oriented in a north-south orientation at about 0°. These terraces are a shorter than the east-west oriented terraces at about 35 meters in length and have a similar width of about 10 meters.

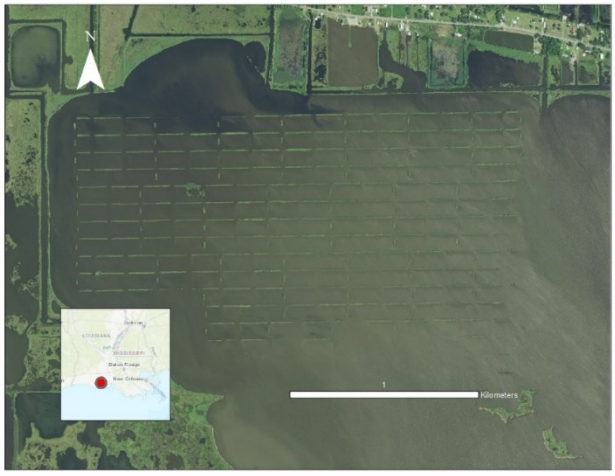

Figure 4.1 Miller property in southern Louisiana. Terraces at this site exhibit a semi-box pattern with linear ridges predominately oriented north to south and smaller terraces oriented north to south. Large areas of open fetch exist to the south and east of the terrace field.

RESULTS

SEDIMENT CRITICAL SHEAR STRESS

The threshold for erosion for sediments throughout the Miller property was calculated for the marsh terraces and the marsh platform from observed sediment sample wet bulk density values (Table 4.1 and Figure 4.2) (Mehta, 1988). Descriptive statistics from table 4.1 show that differences exist between sediment density and sediment shear strength in sediments from the marsh platform and constructed terraces.

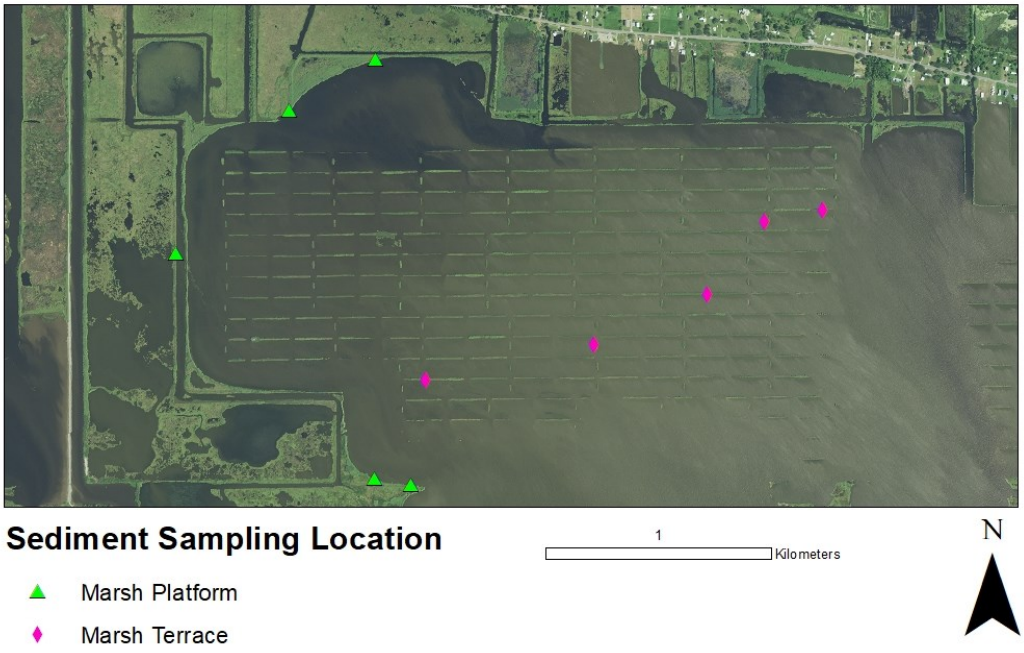

Figure 4.2 Sediment sampling locations at the Miller property. Green triangles represent marsh platform sample locations and the pink diamonds represent marsh terrace sample locations.

Table 4.2 Miller site descriptive statistics of sediment density and threshold for erosion

Location	n	Density Mean (g/cm^3)	Mean τcr (N/m^2)	Variance (N/m^2)	Max τcr (N/m^2)	Min τcr (N/m^2)
Platform	25	1.20	0.200	0.110	0.404	0.053
Terrace	25	1.48	0.481	0.173	0.887	0.311

Mean values for the threshold for erosion at terraces are over twice the value observed are marsh platform sediments. Observed marsh terrace sediments typically exhibited lower concentrations of organic content with very little visible plant matter. Conversely, marsh platform sediments typically included high concentrations of organic matter with visible root systems and dead plant matter commonly visible in the sample. Notably, the mean bulk density

values for sampled marsh terrace sediment are high enough to preclude the penetration of root systems based upon the results of Correa et al., (2019). Correa et al. (2019) was found that clayey sediments with densities of 1.47 g/cm^3 prohibited root systems from penetrating while, sandy sediments do not inhibit root system penetration until about 1.85 g/cm^3. Many of the bulk density values recorded from marsh terraces exceed the ability for root systems to penetrate which is consistent with field observations that show root systems to be absent sediments with recorded values above 1.47 g/cm^3. Marsh platform sediments never exceeded the threshold to inhibit plant root systems from penetrating with a maximum density observed at 1.404 g/cm^3. This value supports the observations of significant plant matter at each of the marsh platform sample locations. Figure 4.3 shows sub-sample with significant plant matter.

Figure 4.3 Sub-Sample of sediment taken from the marsh platform at the Miller property. Sample exhibits lots of organic material and dead plant matter. Root systems and dead biomass make up most of the volume of sediment.

Figure 4.4 shows sample with high clay content retrieved from a marsh terrace. Variance in sediment strength at the marsh platform and marsh terraces indicate that for each, the observed strengths across multiple samples were quite consistent.

Figure 4.4 Sub-sample taken from marsh terrace which exhibits properties relatable to sediments with high clay contents. No visible plant matter or high concentrations of organic material observed in this sample.

WAVE SHEAR STRESS AND FETCH

Four ADCP instruments recorded wave conditions hourly at the study site between Nov 1, 2018 and April 9, 2019. Each of the instruments were strategically placed so that hydrodynamic conditions within and adjacent to the marsh terraces could be captured (Figure 4.5). Wave orbital shear stress was calculated utilizing equations 3.1-3.6 from the time series of data output from the ADCP instruments.

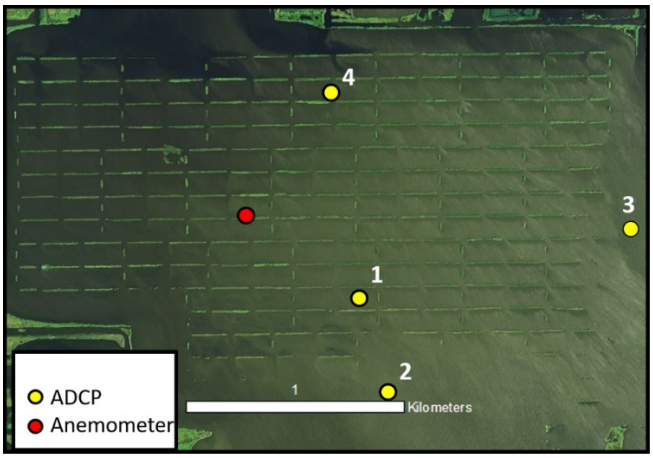

Figure 4.5 Map detailing the placement of ADCP instruments and the placement of the field anemometer. Instruments 1 & 4 are located within terrace cells while, instruments 2 & 3 are out of the terrace field as boundary condition instruments.

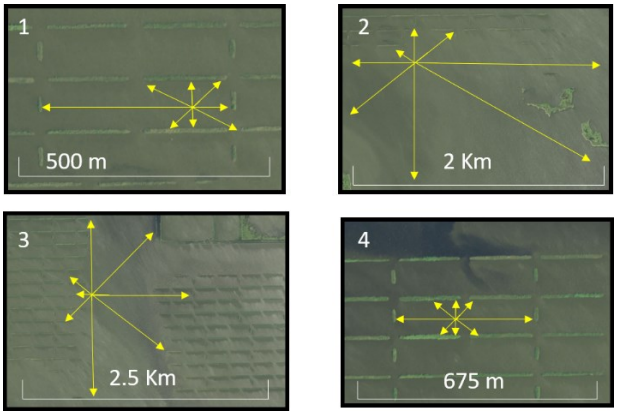

Figure 4.6 Conceptual diagram illustrating fetch at each of the deployed intruments. Yellow rays represent cardinal and ordinal directions of fetch based on distance to immediate structure. Instruments 1 & 4 are located interior to the marsh terraced field while, instruments 2 & 3 are positioned as boundary instruments to observe larger fetches outside of the terraces influence.

ADCP 1 was located in the southern portion of the interior of the marsh terrace field at the Miller study site. The potential fetch exposure for ADCP 1 in the cardinal and ordinal directions is limited by the surrounding terraces and is approximately 90 meters to the north and

south, and 330 meters to the east and west (Figure 4.6). The erosional threshold for marsh terrace sediments was never exceeded by waves observed at this location. Spikes in observed shear stress observed at this instrument occur concurrently with spikes in shear stress observed at the other three instruments indicating a consistent source of stress across the study area.

ADCP 2 was located on the southern perimeter of the study site approximately 300 meters south of the southernmost marsh terraces. Potential fetch at this instrument varies greatly depending on the direction of the wind. The northern to southern directions observe fetch that ranges from 2-2.5 km while eastern to western fetch is about 2 km (Figure 4.6). The erosional threshold for marsh platform and terrace sediments at this instrument was exceeded 52 times during the deployment. This resulted in the threshold for marsh platform being exceeded 31% of the total duration of the deployment and 5.8% of the duration for marsh terraces. When the threshold for erosion is exceeded at this instrument varying degrees of stress are observed. Often the threshold is surpassed by a factor of 2 or more. The 52 periods when the threshold for sediment erosion was exceeded by wave conditions at this site were cyclic in nature (occurring every 3-5 days) and showed a notable consistency with periods of cold front passage. Passing storms are larger synoptic events that exert stress for extended periods before and after storm passage. Before storm passage often a day of strong southernly winds blew winds that resulted in stresses exceeding the threshold for erosion. The passage of the storm resulted in the switching of wind direction to the north with winds typically in greater magnitude for multiple days. Large fetches in the northern and southern directions at this instrument lead to elevated stress as winds blew predominately out of the north and south when strong storms passed through the area.

ADCP 3 was located on the perimeter of the study site approximately 200 meters east of the eastern boundary of the marsh terrace field. Potential fetch at this instrument varies

depending on the direction in which the wind blows. In the northern to southern directions the fetch is 1.7 km and fetch in the eastern and western directions is 0.5 km (Figure 4.6). The calculated stress at this instrument is very similar to the conditions observed at ADCP 2. The erosional threshold for marsh platform and terrace sediments was exceeded at this instrument 48 times during the deployment. This resulted in the threshold for marsh platform being exceeded for 28% of the total duration of the deployment and 12.2% of the duration for marsh terrace. The magnitude to the stress varied as the threshold was crossed but most often the threshold was exceeded by a factor of 2. The 48 periods when the threshold for sediment erosion was exceeded by wave conditions at this site were cyclic in nature (occurring every 3-5 days) and showed a notable consistency with periods of cold front passage.

ADCP 4 was located in the northern portion of the interior of the marsh terrace field at the Miller study site. The potential fetch exposure for ADCP 1 in the cardinal and ordinal directions is limited by the surrounding terraces and is approximately 90 meters to the north and south, and 330 meters to the east and west (Figure 4.6). The erosional threshold for marsh terrace and platform sediments was never exceeded, or even approached, by waves observed at this location.

SHEAR STRESS

Observed wave shear stress conditions for the duration of the deployment are summarized in Table 4.2 and figure 4.7. Wave shear stress observations at ADCP 1 were quite low for the duration of the deployment, rarely rising above 0 and only reaching a maximum of 0.127 N/m^2. Similar conditions were observed at ADCP 4, where observed wave shear stress also rarely rose above 0 and only reached a maximum of 0.17 N/m^2. Conversely, wave shear stress observations at ADCP 2 and ADCP3 were substantially higher with frequent cyclic

(occurring every 3-5 days) spikes above the threshold for marsh terrace and platform sediment erosion. For the duration of the deployment, the mean wave shear stress observed at ADCP 2 was 0.1635 N/m^2 and the mean wave shear stress observed at ADCP was 0.1941 N/m^2 (Table 4.2)..

Table 4.3 Descriptive statistics of calculated wave orbital shear stress at each ADCP instrument in N/m2

Instrument	τ_{0w} min	τ_{0w} max	τ_{0w} mean	τ_{0w} variation
ADCP 1	9.2×10^{-5}	0.1273	0.0053	0.0078
ADCP 2	0.0003	1.4243	0.1635	0.1877
ADCP 3	0.0119	1.3284	0.1941	0.2349
ADCP 4	0.0016	0.1700	0.0216	0.0093

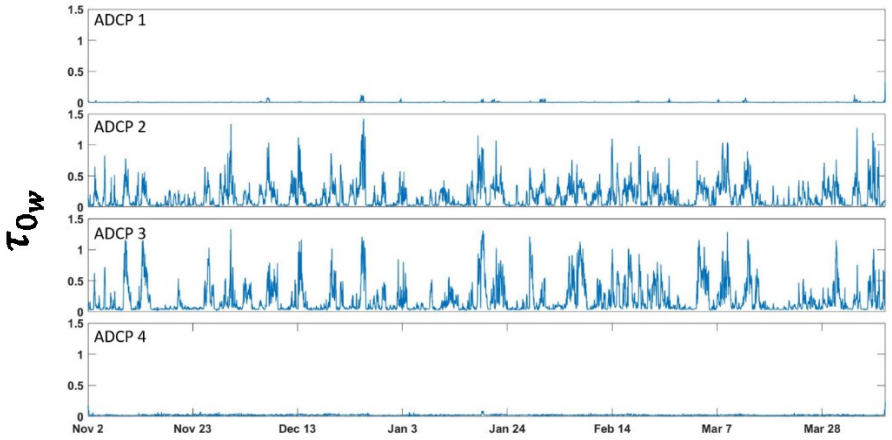

Figure 4.7 Calculated wave orbital shear stress in N/m^2 (Soulsby et al., 1997). Wave shear stress is plotted as a function of time spanning the entire deployment at the Miller property.

Acoustic backscatter intensity for each instrument was plotted as a function of depth and time (Figure 4.8). Relative differences in backscatter intensity were used as a general proxy for

relative difference in suspended sediment concentration (a reasonable assumption for this environment) in order to gain qualitative insight into the dynamics of sediment erosion at each instrument. The four-instruments exhibited consistent cyclic variability in suspended sediment concertation for the duration of the deployment and ADCP 2 and 3 consistently exhibit higher values than ADCP 1 and ADCP4. Notably, higher backscatter intensities, and therefore potentially higher concentrations of suspended sediment, are observed at all instruments to be coincident with higher energy wave events at all locations, even if the local wave conditions do not exceed the threshold for sediment erosion.

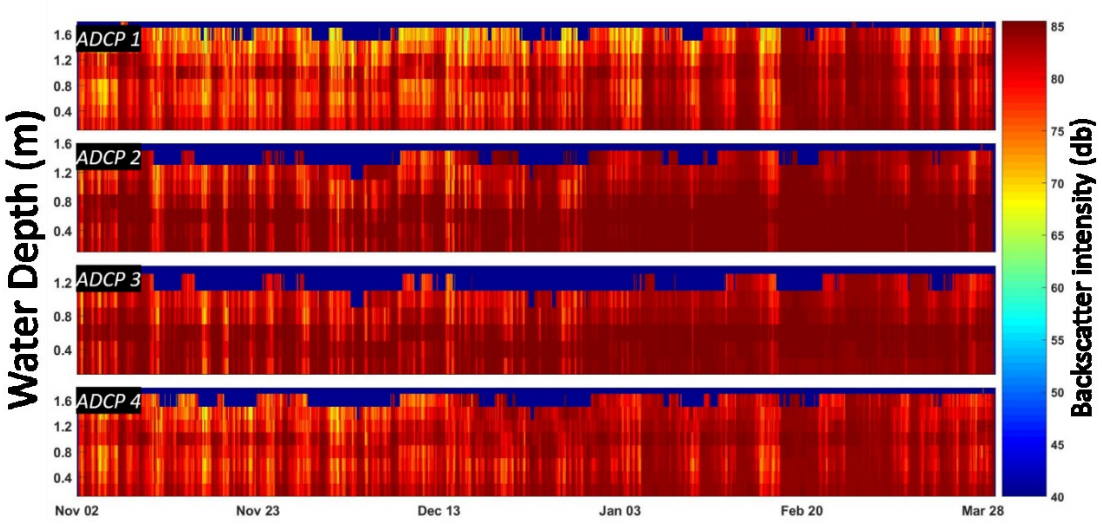

Figure 4.8 Acoustic backscatter for each ADCP instrument plotted as a function of time and depth. Blanked out cells at the top of the plots indicate the water level at the moment in time. Color bar represents observed backscatter intensity with darker red colors signaling high backscatter and blue indicating less.

METEOROLOGICAL CONDITIONS

The Miller deployment occurred mostly during the winter months of 2018-2019. From November 1st, 2018 to April 9th, 2019 the passage of 30 cold front events was observed through

NOAA surface analyses charts. The frequency of the frontal passages occurred at a rate of about once every 5.4 days. Each individual passing front demonstrated varying degrees of intensity, Distinct changes in wind velocity and direction consistent with the passage of strong winter storms that occur regularly over the Gulf Coast region (Guo and Li, 2020), were observed as each front approached and passed the study site.

One of the most notable features of the passage of a cold front storm was the rapid change in wind pattern directions and duration of the event. The cold front passage from November 25th, 2018 for example, demonstrated prolonged duration that exhibited strongly opposed wind directions (Figure 4.9). The pre-frontal portion of the storm is characterized by moderate wind velocities (8 m/s) blowing from the south with a distinct change to winds blowing out of the north as the storm passes and transitions into the post frontal phase of the storm with high velocity (12 m/s) winds persisting for an extended duration (4 days). Given enough fetch, these events could generate high stress from waves in observed wetland environments. The described pattern was consistent across all observed frontal systems except for one frontal system that was observed to pass with a westward trajectory.

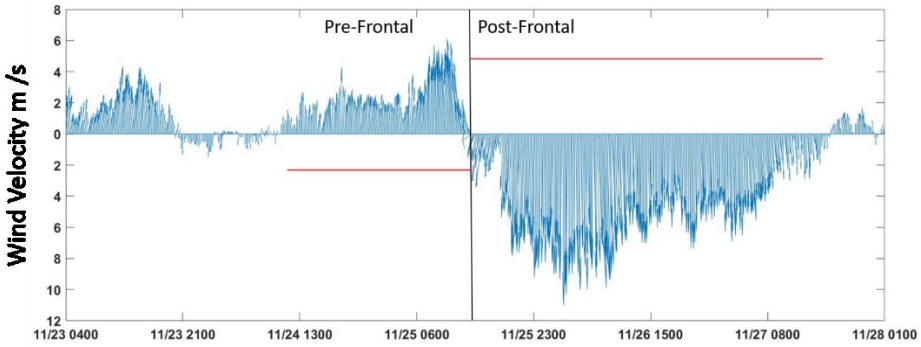

Figure 4.9 Time series data of wind direction and velocity during the cold front passage on November 25th, 2019. The passage is notable as it is a long-lived event starting with the arrival of the pre-frontal portion of the storm on November 24th with the storm ending 4 days later November 28th. This diagram also illustrates the diagnostic wind patterns of the cold front passage where pre-frontal winds blow from south and post-frontal winds make a quick distinct change to the north.

Figure 4.10 is a wind rose diagram that plots the frequency of observed wind direction and velocity. The primary wind directions during the deployment were bimodal with a distinct northeasterly and southeasterly component, particularly for winds of the highest velocity.

.

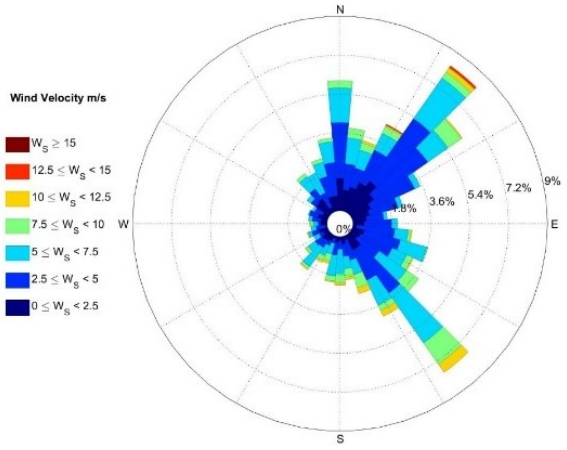

Figure 4.10 Wind rose of all the wind data recorded during the Miller deployment. Wind data is binned by direction and the magnitude represents the frequency and velocity indicated by color.

DISCUSSION

The deployment at the Miller property captured the passage of multiple storm events with sufficient wind velocity and duration to produce erosive waves. The magnitude of the resultant bed shear stresses varied across the study site, with higher magnitudes observed at the fetch exposed perimeter of the marsh terrace sites and lower magnitudes observed in the interior of the marsh terrace site (Figure 4.11). Specifically, erosive waves were observed at ADCP 2 and 3 when winds were blowing from the direction with maximum fetch exposure at each instrument. During periods when these erosive waves were observed at ADCP 2 and 3, no erosive waves were observed at ADCP 1 and 4. Given the proximity of all four instrument locations, it can be assumed that they were exposed to equivalent wind velocity and duration. Therefore, the substantial difference in calculated bed shear stress among the locations can be attributed to differences in fetch (based upon equation 2.1). These observations indicate that marsh terraces at

the study site are serving as an effective means of mitigating wave induced erosive stress through the disruption of fetch. This result directly addresses hypothesis 2 and indicates that marsh terraces can alter hydrodynamic processes in a manner that makes them effective as a marsh resonation method.

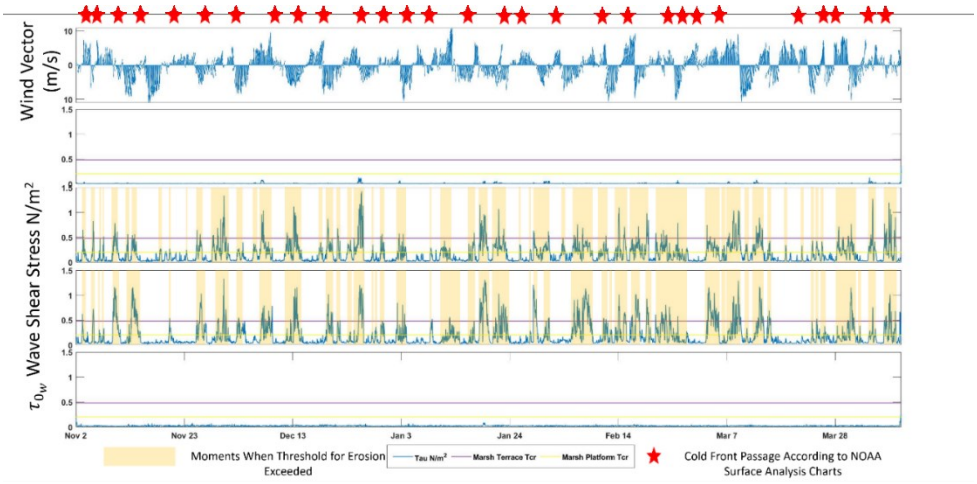

Figure 4.11 Time series plots of wind vectors and calculated wave orbital shear stress at each instrument during the entirety of the Miller deployment. Red stars in this figure highlight the moments when cold front passages were observed according to NOAA surface analyses charts. Yellow boxes that are present in plots of wave shear stress highlight moments when the threshold for erosion was exceeded at the marsh platform during the deployment. Threshold for erosion for terraces indicated by purple line (0.4085 $N/m^{2)}$ and marsh platform yellow line (0.2002 N/m^2).

Published surface analyses charts indicate that during the Miller deployment 30 frontal passages occurred. Figure 4.8 indicates that the passages of frontal systems is roughly cyclic with a frequency of 5.4 days. While, there is not a direct correlation between the passage of cold fronts and erosive condition, there does appear to be a strong association between them.

A rose diagram of observed winds during the periods when wave shear stress exceeded the threshold for erosion indicates the frequency of wind directions and velocities that responsible for marsh erosion (figure 4.12). The observed distribution of wind directions during

periods of erosion is bimodal. Winds predominantly blew out of the north and southeast directions when the erosional threshold was exceeded. These two directions coincide with the known and observed wind patterns that are associated with the passage of strong cold fronts. The southeast winds are associated with the pre-frontal stage of a cold front. This is a period associated with observed local water elevation rise as surging winds from the south push water inland and given enough fetch will produce waves with enough strength to erode sediments. As cold front systems pass there is a rapid change in wind direction and generally an increase in wind velocity as shown in Figure 4.9. The north winds that blow as a cold front storm passes typically blow with the greatest intensity. As cold front systems pass the southernly wind shift to the north which transport recently eroded sediments. Winds from the east and west were not observed to create waves with shear stresses greater than the critical threshold for erosion. The absence of the winds in these directions emphasizes that cold front passage and their associated wind fields are the main source of erosive shear stress in these environments (hypothesis 1).

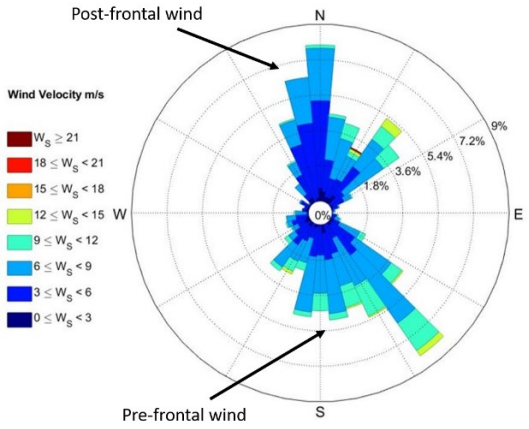

Figure 4.12 Distribution of wind velocity and direction for periods when the threshold for erosion was exceeded by wave orbital shear stress at the marsh platform.

Consideration of individual wave events yields further insight into the erosive processes associated with cold front passage at each instrument (Figure 4.13). Given that wind fields are synoptic processes and are generally uniform across small spatial domains the contribution of fetch to wave energy can be surmised from equation 2.1. This is emphasized by comparison of conditions at an instrument with large fetch exposure (ADCP 3) and small fetch exposure (ADCP 1) during the passage of a strong cold front on November 25th, 2018. During this event, prefrontal northerly winds with a velocity of ~ 5 m/s rapidly become southerly and increase in velocity to ~10 m/s. ADCP 1 ,which has fetch exposure of ~ 90 m to the north and south experiences substantially lower wave shear stress and suspended sediment concentrations than ADCP3, which has fetch exposure in excess of 2.5 km to the north and south. Acoustic backscatter intensity values, which are a qualitative proxy for relative suspended sediment concentration, remain relatively low and both ADCP1 and ADCP 3 prior to the passage of the cold front and both increase rapidly after the passage of the cold front. This increase at both locations, despite the fact that waves at ADCP 1 are not sufficient to erode sediment suggest that higher concentrations of suspended sediment being generated at locations in the study sites where wave conditions are sufficient to erode sediments (e.g. ADCP 3), is rapidly diffusing throughout the study site.

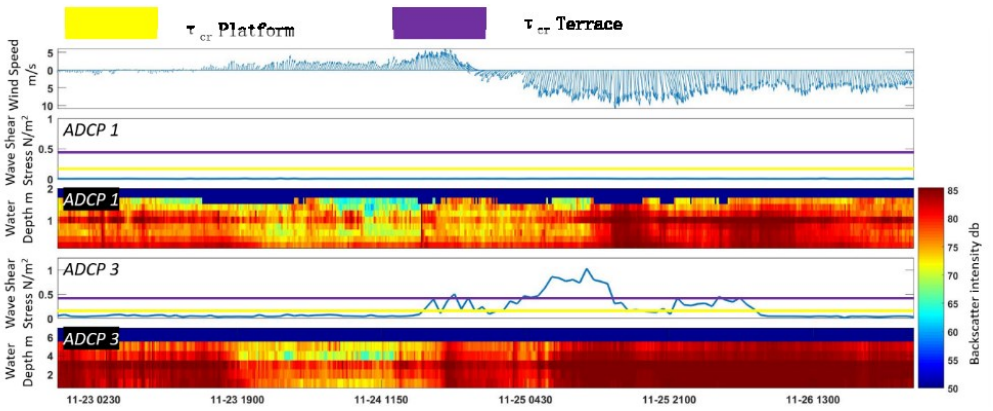

Figure 4.13 Comparison of ADCP 1 and 3 during a single storm passage. For the same wind conditions ADCP shows relatively longer periods of lower backscatter intensity. During storm passage ADCP 3 observes significantly more stress than ADCP 1 and the backscatter at ADCP 3 instantly observes an intensity increase. Calculated thresholds for erosion for marsh terrace (0.481 N/m2) and marsh platform (0.200 N/m2) indicated by purple and yellow lines.

CHAPTER V

MIAMI DEPLOYMENT

INTRODUCTION

The Miami property is located in Chenier plain of coastal Louisiana (29.657041, -92.615368) (Figure 5.1). The property lies just south of highway 82 and lies about 7 km south of White Lake and about 40 km east of Grand Chenier Louisiana. From April 10th, 2019 to September 3rd, 2019 (146 days) four ADCP instruments and an anemometer were deployed to capture meteorological and hydrodynamic conditions at this site. Additionally, sediment samples were subsequently collected on February 2, 2019 to use in the calculation of terrace and marsh palatiform bulk density.

The area of the Miami property is approximately 1.75 km^2 with marsh platform immediately surrounding the northern, southern, and eastern boundaries and a transportation canal on the western edge of the site. The terraces at this site are constructed in a chevron pattern (Figure 5.1). The azimuthal orientation of each chevron limb alternates between 60° and 300°. These terraces are approximately 300 meters long; although, their length can vary due to the presence of marsh platform. Terrace width varies slightly across the study site, but the mean width is about 10 meters across.

Figure 5.1 Map of Miami site in chenier plain in coastal Louisiana. This site is characterized by chevron shaped terraces and semi-chevron shapes.

The terraces at the Miami property are surrounded by marsh platform on the northern, southern, and eastern boundaries and a transportation canal lies to the west of the site. The individual terraces at this site are constructed in a chevron shape. Terrace length varies throughout the site depending on whether the terrace is a completed chevron shape or rather just a linear limb that is not connected to another limb. Full chevron terraces are about 300 meters in length with a width of about 10 meters. The total area of the Miami site is 1.75 km^2.

RESULTS

CRITICAL SHEAR OF SEDIMENTS

The threshold of erosion for sediments throughout the Miami property was calculated for the marsh terraces and the marsh platform (natural marsh wetlands) from observed sediment sample wet bulk density values (Table 5.1 and Figure 5.2) (Mehta, 1988). Descriptive statistics from table 5.1 show that differences exist between sediment density and sediment shear strength

in sediments from the marsh platform and constructed terraces. Marsh platform sediments were observed visually to exhibit more organic material, less clay content, and in general plant matter that overall contributed to a lower density. Marsh terrace sediments however, visually exhibited higher clay content, low organic material, and higher clay contents. These differences are largely attributed to the depositional nature at these features. Decaying plant matter near the marsh platform contribute to sediments with an overall low density while, no major sediment input sources contribute fine grained material. Fine grained material that is eroded supplies the major sediment input for sediments at marsh terrace locations. This fine grained material contributes to the higher wet bulk density observed at the testing locations.

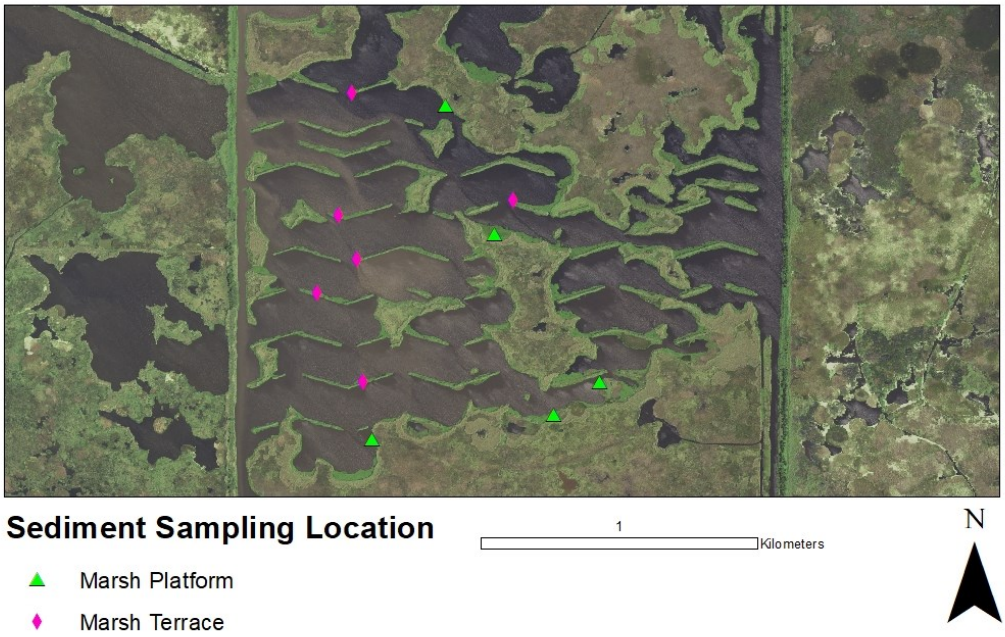

Figure 5.2 Sediment sampling locations at the Miami property. Green triangles represent samples taken on the marsh platform and pink diamonds represent samples taken on marsh terraces.

Table 5.2 Miami site descriptive statistics of sediment density and threshold for erosion

Location	n	Density Mean (g/cm^3)	Mean τcr (N/m^2)	Variance (N/m^2)	Max τcr (N/m^2)	Min τcr (N/m^2)
Platform	25	1.187	0.187	0.057	0.253	0.073
Terrace	30	1.519	0.519	0.153	0.880	0.360

Mean values for the threshold for erosion at terraces are over twice the value observed at marsh platform sediments. Marsh terrace sediments typically exhibited lower concentrations of organic content with very little visible plant matter. Conversely, marsh platform sediments typically included high concentrations of organic matter with visible root systems and dead plant matter commonly visible in the sample. Notably, the mean bulk density values for sampled marsh terrace sediments are high enough to preclude the penetration of root systems based upon results of Correa et al. (2019) who found that clayey sediments with densities of 1.47 g/cm^3 prohibited root systems from penetrating while, sandy sediments do not inhibit root system penetration until about 1.85 g/cm^3. Many of the bulk density values recorded from marsh terraces exceed the ability for root systems to penetrate which is consistent with field observations that show root systems to be absent sediments with recorded values above 1.47 g/cm^3. Marsh platform sediments never exceeded the threshold to inhibit plant root systems from penetrating with a maximum density observed at 1.404 g/cm^3. This value supports the observations of significant plant matter at each of the marsh platform sample locations. Figure 5.3 shows saturated clay that is devoid of plant matter with vegetation only existing in the aerial portion of the sediment.

Figure 5.3 Saturated clay sediment that is a part of a marsh terrace. No plant matter or organic content observed in the sediment. Above the sediment on the terrace a small horizon of organic material exists for vegetation to grow.

WAVE SHEAR STRESS AND FETCH

Four ADCP instruments recorded wave conditions hourly at the study site between April 10, 2019 and Sep 3, 2019. Instrumentation at this site was strategically placed so that hydrodynamic conditions could be captured within the terraced field (Figure 5.4). Wave orbital shear stress was calculated utilizing equations 3.1-3.6 from the time series of data output from the ADCP instruments.

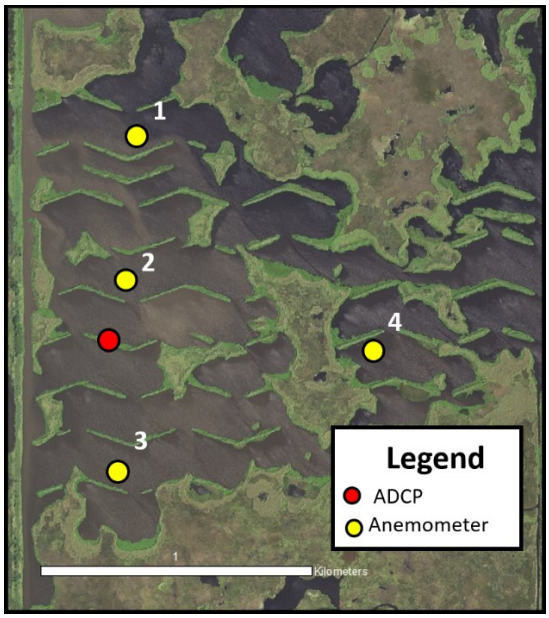

Figure 5.4 Map of ADCP instrument locations and anemometer location within the Miami property.

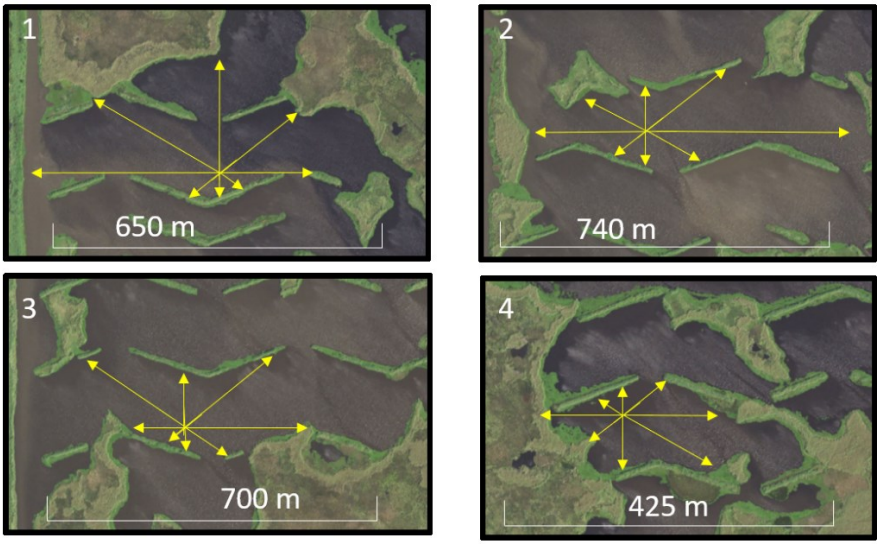

Figure 5.5 Conceptual diagram illustrating fetch at each of the deployed instruments. Yellow rays represent cardinal and ordinal directions of fetch based on distance to immediate structure.

ADCP 1 is located at the north western corner of the Miami site. Fetch for this instrument is limited by a marsh terrace immediately to its south with about 150 meters of fetch to the north and south and roughly 300 meters to the east and west (Figure 5.5). The erosional threshold for marsh platform was only exceeded 1.2% of the time during the deployment. The erosional threshold for the marsh terraces was never exceeded. The moments when the threshold was crossed were sporadic and seemingly random.

ADCP 2 is in the central western portion of the Miami site. Fetch at this instrument is limited by terraces to the north and south with 150 meters of fetch and 500 meters of fetch to the east and west (Figure 5.5). The erosional threshold for marsh platform was exceeded 0.8% of the time during the deployment. The erosional threshold for marsh terraces was never exceeded. The moments when the threshold was crossed were sporadic and seemingly random.

ADCP 3 is in the south western portion of the Miami site. Fetch at this instrument is limited by terraces to the north and south with 150 meters of fetch and 200 meters of fetch to the east and west (Figure 5.5). The erosional threshold for marsh platform was exceeded 1% of the time during the deployment. The erosional threshold for marsh terraces was never exceeded. The moments when the threshold was crossed were sporadic and seemingly random.

ADCP 4 is in the eastern portion of the Miami site. Fetch at this instrument is limited by terraces to the north and south and marsh platform to the east and west. Fetch is 150 meters to the north and south directions and 250 meters to the east and west directions (Figure 5.5). The threshold for erosion was exceeded 0.82% of the time during the deployment. The erosional threshold for marsh terraces was never exceeded. The moments when the threshold was crossed were sporadic and seemingly random.

In general, the geometry of this site restricts fetch due to the intermingling growth of marsh platform with the placement of the chevron shaped marsh terraces. The site does not allow for the placement of any instruments to be considered boundary condition or to be placed into relatively open water with lots of exposed fetch. It is observed that the marsh platform in this case segments fetch to a similar degree as the terraces.

Observed shear stress conditions for the duration of the deployment are summarized in Table 5.2 and Figure 5.6. Wave stress at all of the instruments exceeded the threshold for erosion only for sediments of the marsh platform. The nature of the stress spikes was seemingly random and for very short durations on average representing only 1% of the observed time at each instrument. The only significant event recorded was the passage of Hurricane Barry on July 13th, 2019.

Table 5.3 Descriptive statistics of calculated wave orbital shear stress at each ADCP instrument in N/m2

Instrument	τ_{0w} min	τ_{0w} max	τ_{0w} mean	τ_{0w} variation
ADCP 1	0.0027	0.4055	0.0106	0.0234
ADCP 2	0.0098	0.4997	0.0457	0.0314
ADCP 3	0.0071	0.6839	0.0596	0.2349
ADCP 4	0.0112	0.2641	0.0363	0.0137

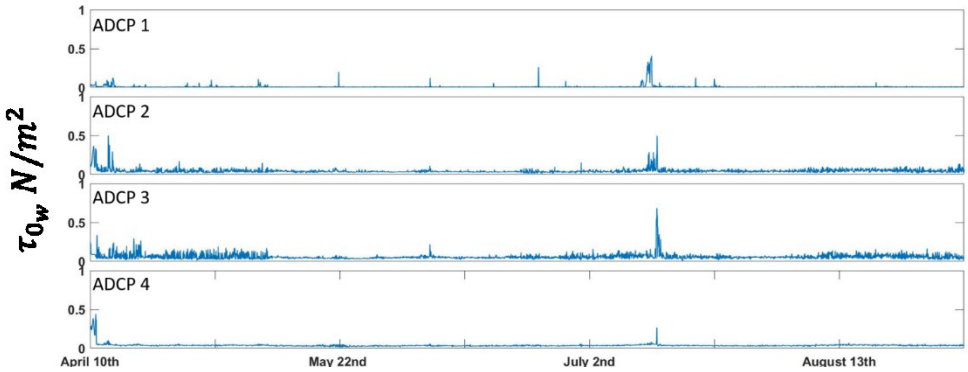

Figure 5.6 Wave orbital shear stress recorded at each ADCP instrument through the entirety of the field deployment April to September 2019. Wave orbital shear stress parameterized as N/m^2.

ACOUSTIC BACKSCATTER

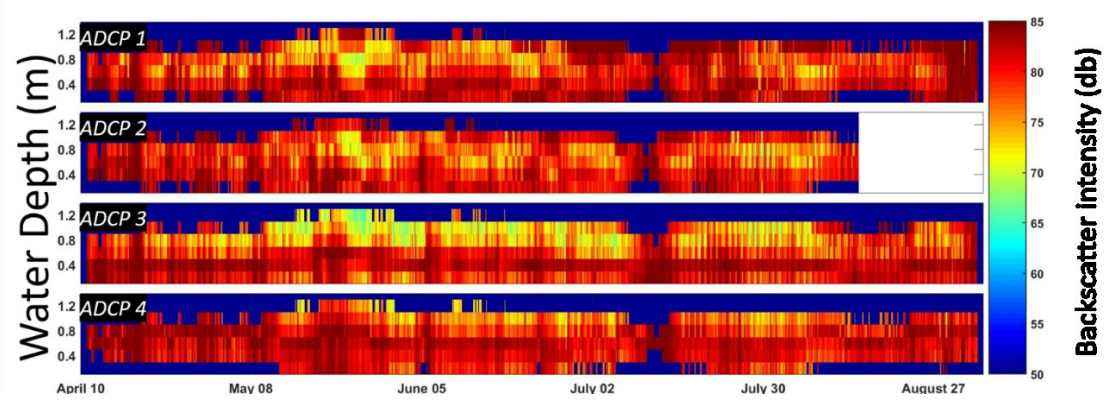

Figure 5.7 Acoustic backscatter for each ADCP instrument plotted as a function of time. Blanked out cells at the top of the plots indicate the water level. Color bar represents observed backscatter intensity with darker red colors signaling high backscatter and blue indicating lower intensity.

Acoustic backscatter intensity for each instrument was plotted as a function of depth and time (Figure 5.7). Relative differences in backscatter intensity were used as a general proxy for relative differences in suspended sediment concentrations (a reasonable assumption for this

environment) in order to gain qualitative insight into the dynamics of sediment erosion at each instrument. The four-instruments exhibit consistent cyclic variability in suspended sediment concertation for beginning months of the deployment as the winter storms season is ending. The summer months observe a general relative decrease in intensity at all of the instruments until the passage of Hurricane Barry on July 13th, 2019. Notably, the backscatter increases at all instruments and the instruments also recorded a significant water level drop of about 30 cm. This was attributed to the strong winds blowing to the southeast and then to the southwest as Hurricane Barry passed through the study area. Therefore, stressors during this deployment seem to be the ending of the cold front passages in the early spring and the lone passage of Hurricane Barry.

METEOROLOGICAL CONDITIONS

The Miami deployment occurred during the summer months of 2019 from April 10th-September 3rd for a total of 146 days. During the time span 10 cold fronts were through NOAA surface analysis charts and the single passage of Hurricane Barry was also observed on July 13th, 2019. Anemometer data collected during this deployment was compromised by local vegetation growing onto instrument and disrupting data collection about a third of the way through the deployment (Figure 5.8). Therefore, local climatological data was downloaded from the closest NOAA weather station which was the weather station at Abbeville regional airport which is 62 km away from the study site (Figure 5.9).

Figure 5.8 Deployed anemometer that was overgrown by local marsh vegetation. Significant error was determined to exist in the data, so the anemometer's data was not used for analysis of the Miami deployment.

Figure 5.9 Map showing proximity of Miami site to the NOAA weather station at the Abbeville regional airport.

Wind fields during the deployment were predominately blowing out of the south. These wind patterns are typical of convective wind patterns blowing onshore (Figure 5.10). Storm

passage is observed during the beginning of the deployment but, as summer months pass much of the observed wind intensity dissipates.

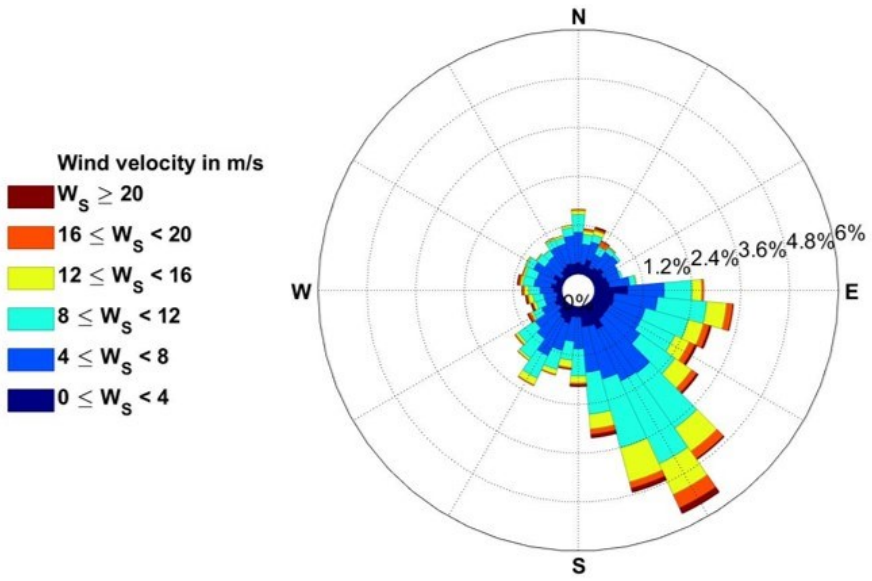

Figure 5.10 Wind rose of Abbeville airport weather station. Most wind is observed blowing from the south which coincides to typical wind patterns in the coastal Louisiana area from convective set up.

DISCUSSION

The deployment at the Miami property captured the passage of only a few storm events with sufficient wind to produce erosive waves (Figure 5.11). Wave shear stress across the study site was relatively uniform as it was never present for sustained durations at any instrument. The highest stresses were observed when Hurricane Barry made landfall which was observed which resulted in a spike in stress and also drop in water levels by 30 cm. The geometry of the marsh terraces in the Miami property were able to segment fetch in effective manner reducing observed stresses as no areas existed with longer fetches to generate erosive waves for sustained durations. The beginning of the deployment captured the winding down of the winter storms as the local

weather began to transition into a calmer summertime pattern. This pattern is much more akin to convective set up leading to offshore winds dominating the weather. Ten cold front passages would be observed via NOAA published surface analysis charts but, did not strongly influence wave shear stress at any of the instruments. The threshold for erosion was exceeded only a few times other than the passage of Hurricane Barry. The uniform geometry of marsh terraces and immediacy of marsh platform result in a marsh pond that is effectively segmenting fetch. ADCP instruments indicate that wave shear stresses were greatest at the northern side of marsh terraces and platform as southernly winds blew with the most frequency. Hypothesis 2 is addressed directly and indicates that marsh terraces perform effectively to alter hydrodynamic processes making marsh terraces an effective restoration method.

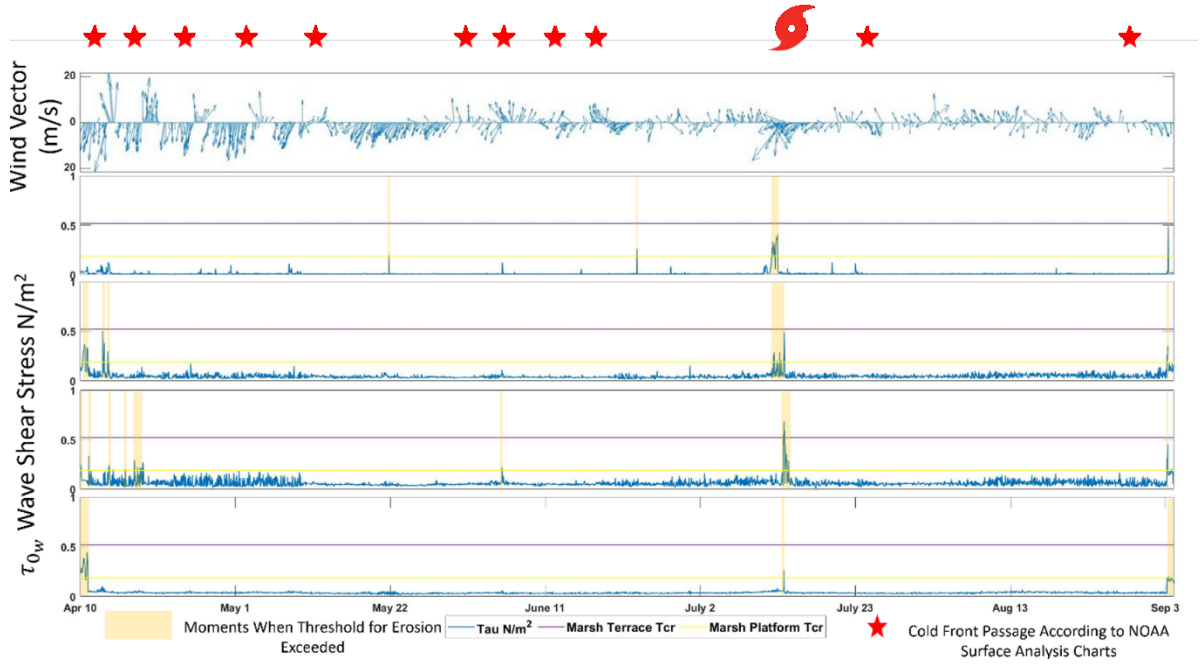

Figure 5.11 Plots of time series data of wind vectors and calculated wave shear stress. Passage of storms are highlighted by stars (frontal passages) and hurricane symbol to signify passing of system. Thresholds for erosion are imposed by purple line for marsh terraces (0.519 N/m^2) and yellow for marsh platform (0.187 N/m^2).

Figure 5.11 outlines a synopsis of the event timing that occurred during the Miami deployment. The calculated wave stress during this deployment is almost nonexistent for much of the span of the deployment. That may be attributed to the general weakening of frontal systems as summertime storm passages are not as intense as their winter counter parts. Hurricane Barry was a strong storm system that had a multiple day influence on the study area and induced substantial erosive stress into the study site. Only July 13th, 2019 Hurricane Barry made landfall and its trajectory passed directly over deployed instruments (Figure 5.12). Associated winds were recorded by the Abbeville NOAA weather station therefore, reported wind speeds and directions are conservative estimates of conditions at the study site, which is further inland. The produced wind velocity and duration that contributed to all four ADCP instruments to record very high stress levels. The threshold for erosion was exceeded during a drop in water levels which may suggest that during this event sediment laden water may have been expelled out of the local area (Figure 5.13).

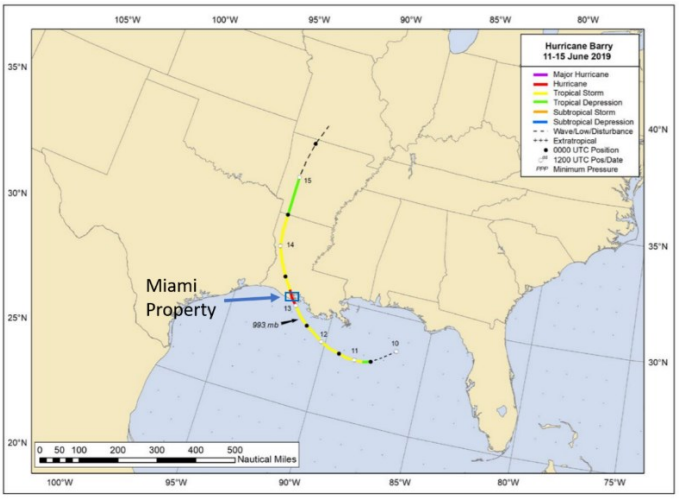

Figure 5.12 Path of Hurricane Barry. Red portion of track signifies hurricane status and is also the portion of the storm that passed directly over. (Adopted and Modified from Cangialosi et al., 2019)

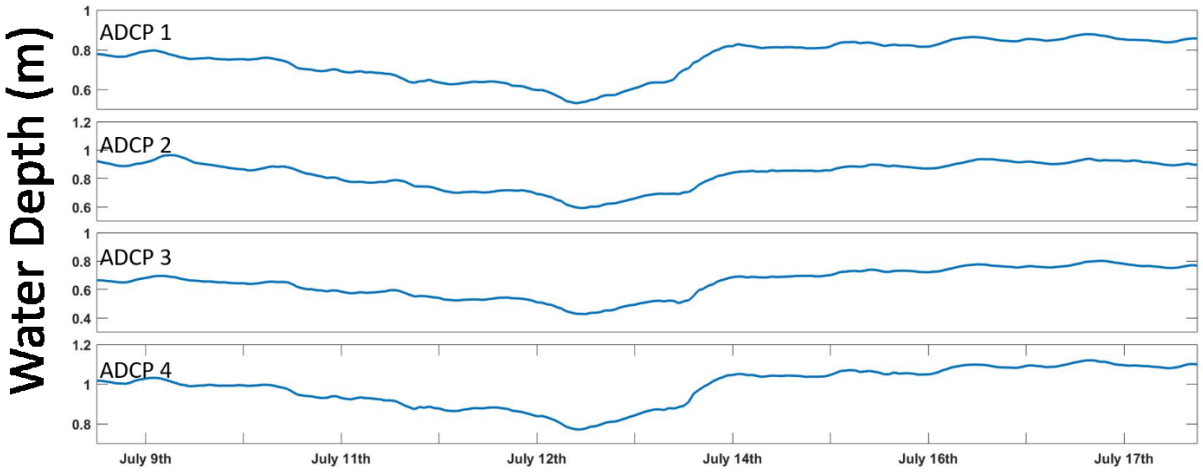

Figure 5.13 Water depth at each ADCP instrument during the passage of Hurricane Barry. Each instrument observes water levels drop during the passage of Hurricane Barry due to strong winds blowing south driving down water levels.

Given the same wind conditions across the study area the passage of Hurricane Barry demonstrates how terraces may perform during a tropical event. Figure 5.14 shows that ADCP3 observed a spike in stress that crosses the threshold for erosion whereas, ADCP 4 did not. This could be attributed to the placement of the ADCP instruments as ADCP 3 was positioned at the southern end of the row while, ADCP 4 was positioned at the northern end of its respective row. What was observed was an increased stress over increasing fetch. Stresses were low at the northern edges of individual marsh terraces, and they grew as winds blow to the south eventually dissipating on adjacent terraces. Acoustic backscatter suggests that this event was particularly stressful as high backscatter intensity is observed at instruments with low and high wave shear stress. Coupled with lowering water levels it is suggested that sediment laden waters were expelled from this local environment resulting in a reduction in the local sediment budget. The lack of significant wave events other than the passage of Hurricane Barry suggests that in general late spring to summer weather patterns produce much less stress than late fall and winter weather patterns. The growth of stress between adjacent terraces suggest that wave energy has to re-generate within this terrace field suggesting that marsh terraces are effective at reducing wave shear stress (hypothesis 2).

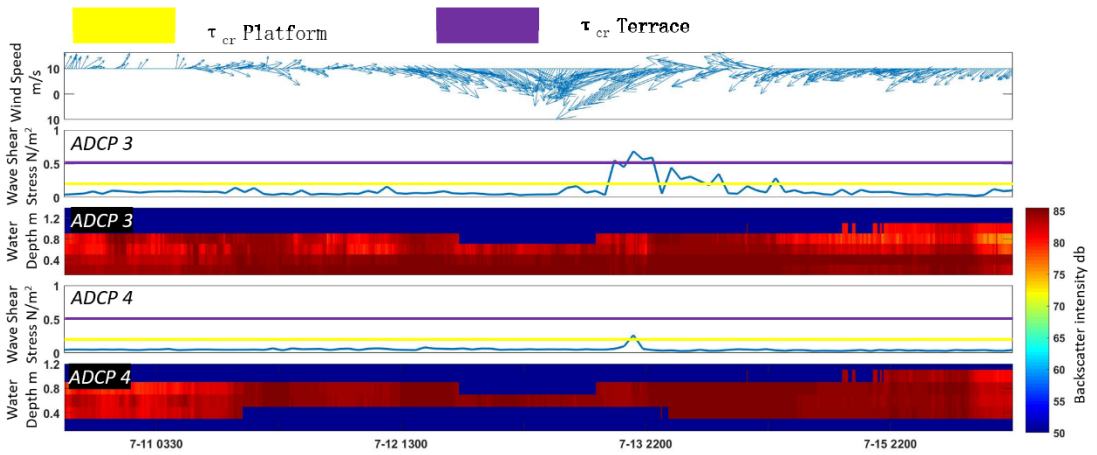

Figure 5.14 Plots that describe the conditions observed at two ADCP instruments during the passage of Hurricane Barry. It is noted that the acoustic backscatter detects the water level drop and that intensity values indicate that significant erosion may be taking place. During the storm passage stress is observed to increase at ADCP 3 that is observed to more fetch compared to ADCP 4.

Generated wind rose diagrams of when the threshold for erosion has been exceeded reveal which winds were present during high energy events (Figure 5.15). The summertime weather pattern observed stresses were predominantly from winds blowing to the south. Particularly, those winds mainly blew from the passage of Hurricane Barry and a few cold front passages.

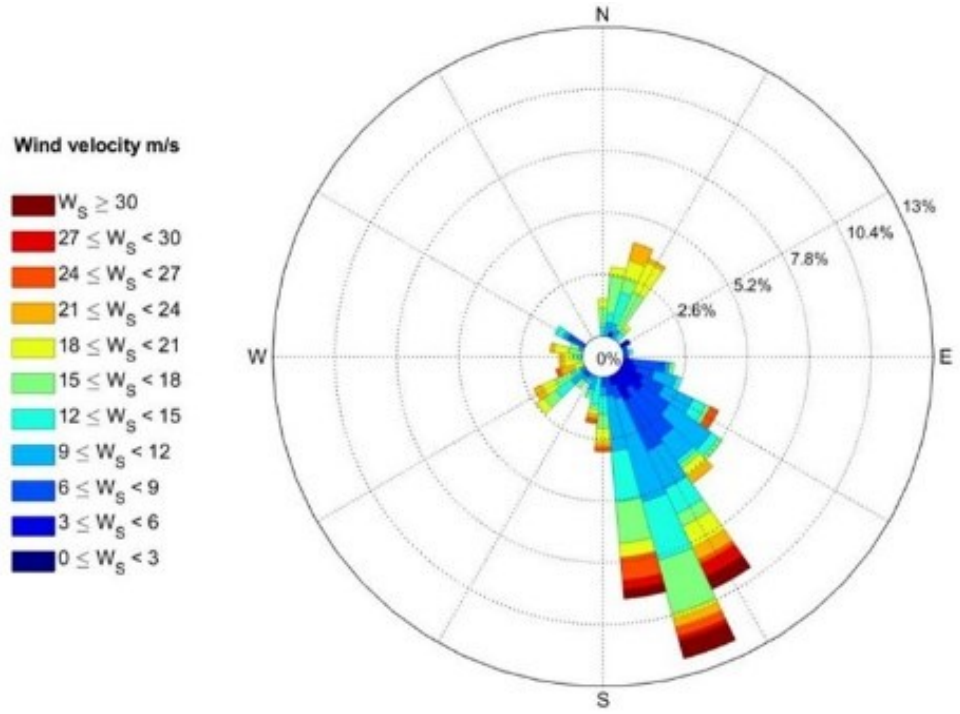

Figure 5.15 Rose of winds that exceeded the threshold for erosion for the marsh platform during the Miami deployment

Given the same meteorological conditions over the study site, the spatial changes in stress suggest a few things about the performance of marsh terraces during summertime months. The geometry of marsh terraces plays a pivotal role with the reduction of fetch which in turn reduces wave shear stress in the marsh ponds. Other than the passage of Hurricane Barry the threshold for erosion during the summer months (May-August) was exceeded sparingly and only for briefly. This suggest that terraces can effectively reduce stress as terrace shape and orientation matter.

Figure 5.15 the wind rose of the meteorological conditions of when the erosional threshold was exceeded is primarily composed of wind from the passage of Hurricane Barry. Basing design of marsh terraces on the data from this deployment is not recommended as

summer cold front systems do not pass with the intensity to produce erosive ways for any meaningful amounts of time. Designing against the passage of a Hurricane may not be recommended either as the infrequency of storm passage and distinct wind patterns make the event to irregular to plan for. If effective placement of terraces is introduced marsh hydrodynamic conditions are likely to be favorable to not eroding sediments.

CHAPTER VI

DISCUSSION

From November 2018 to September 2019 almost 8 months of continuous data were recorded from two proximal marsh terrace sites in the chenier plain of coastal Louisiana. Hydrodynamic observations were used to calculate the shear stress imparted on the bed by wind generated waves. The bulk density of sediment samples collected from the marsh platform and marsh terraces at each site was used to calculate the critical bed shear stress necessary to erode sediment. Metrological observations were used to determine the source of the winds responsible for periods of erosion in each study site. Synthesis of these observations indicate that the winter months at the Miller property study site experienced frequent wind conditions sufficient to potentially erode marsh terraces and the marsh platform. However, the late spring to summer months observed at the Miami study site were much less frequent and less stressful. Additionally, it was determined that the most important parameter in determining whether erosion occurred within each study site was the fetch exposure in the direction of prevailing winds. Finally, it was found that and that cold front generated winds were temporally coincident periods of sediment erosion.

Bulk density analysis of sediment samples indicates that marsh platform sediments are mechanically weaker (.e. lower shear strength) than the adjacent constructed marsh terraces. The calculated relative shear strength of marsh terraces and the marsh platform sediments were consistent between the two study sites. The bulk density of marsh terraces indicates that

vegetation growth may be restricted on these features. This is likely attributable to the mechanical compaction of terrace sediments during construction as well as their higher ratio of clay to organic content. Marsh platform sediments were found to be generally weaker with values that always allow for vegetation to take root. This is supported by observations of abundant root systems, organic matter, and a lower clay content at marsh platform sites.

The result of this investigation, indicate that one of the primary design considerations for marsh terraces should be the direction of cold fronts winds, given their frequent and predictable pattern as well as their demonstrated capacity to generate waves that can erode marsh platform and terrace sediments. Although the second deployment demonstrated that Hurricanes can produce wind field intensities that are equal to or greater that cold fronts, they are not a primary design consideration for marsh terraces because their paths, and therefore associated wind fields are not as consistent or predictable as those of cold fronts. The optimization of marsh terraces should be based upon the most frequent and predictable sources of erosive stress, which this research found to be cold fronts. Given that the erosive potential of waves is a function of fetch, marsh terraces should be oriented to most directly interrupt fetch in the direction of the highest intensity winds, which were observed in this thesis to be pre and post frontal winds. (Figure 6.1). Analyses of cold front associated winds present when the threshold for erosion was exceeded suggest that the optimal marsh terrace orientation for disrupting fetch in the directions of frontal winds are 235°/55° and 270°/90°. The resultant shape would be a chevron shape as indicated in Figure 6.1.

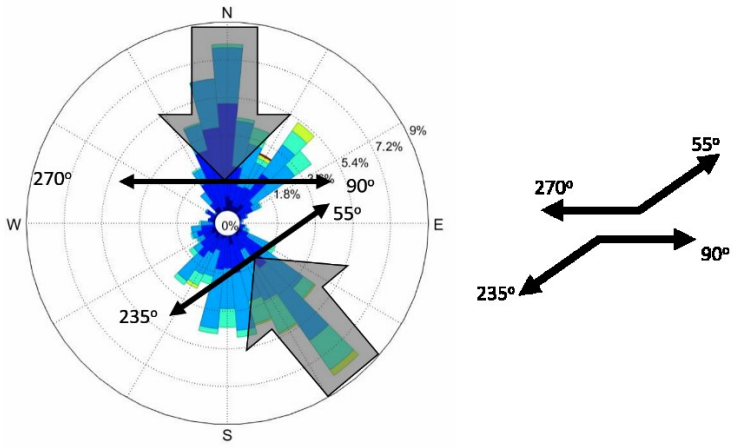

Figure 6.1 Prescribed marsh terrace orientation considering cold front winds (right). Wind rose is representing winds present when the threshold for erosion was exceeded during the Miller of marsh terrace shape based off cold front winds (left).

Figure 6.3 represents a conceptual diagram of what the Miller property might look like if the prescribed design was implemented. Design considerations should not incorporate the wind rose information that was collected during the passage of Hurricane Barry because tropical systems passing through the Gulf Coast are inherently difficult to predict and observed wind fields will be highly dependent on marsh terrace sites position in relation to that storm.

Although a few terrace project sites on the Gulf Coast essentially match this prescribed orientation pattern, most exhibit shapes and orientations that are suboptimal with regard to disruption fetch from cold front generated winds (Figure 6.2). Future efforts to design marsh terrace projects in the Gulf of Mexico should consider the orientation of cold front associated winds and the prescribed orientation for marsh terraces presented in this thesis. Future efforts to design marsh terrace projects in other regions should consider the source of winds that result in the most erosive waves for that region and develop terrace orientations that most effectively interrupt fetch in the direction of those winds.

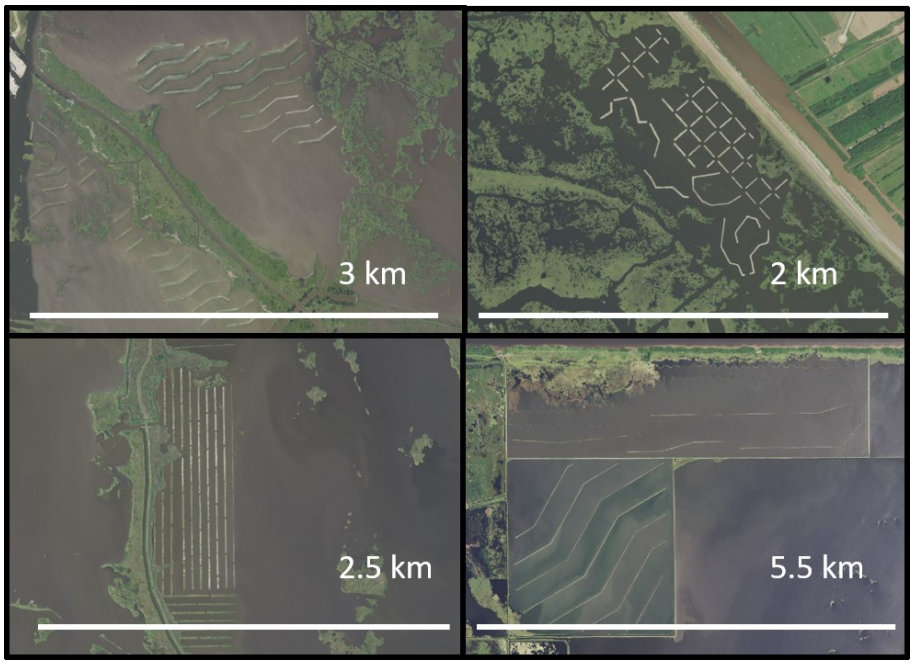

Figure 6.2 Examples of the different designs of marsh terraces across the Gulf Coast that can be compared with prescribed shape and orientation.

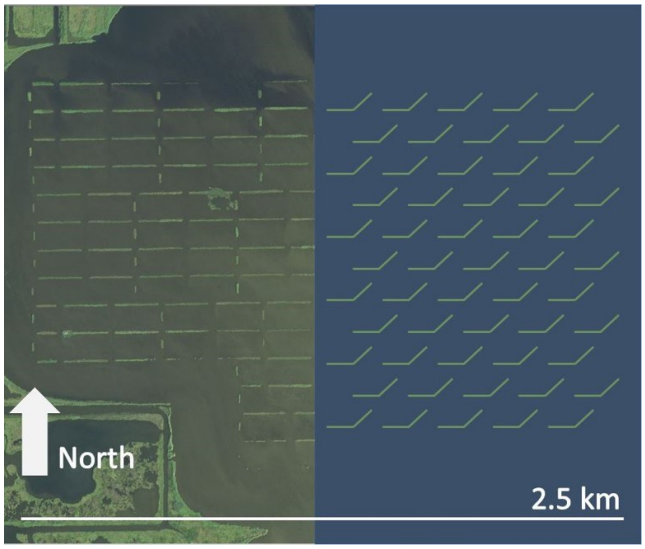

Figure 6.3 Conceptual diagram of marsh terrace orientation and shape. Miller property left side of image and the conceptual terraces on the right side of the image.

REFERENCES

Ahrens C. D., Henson, R. 2019. Meteorology today: an introduction to weather, climate, and the environment, 12th edn. Cengage Learning, Boston, MA

Amos, C. L., Bergamasco, A., Umgiesser, G., Cappucci, S., Cloutier, D., DeNat, L., Flindt, M., Bonardi, M., and Cristante, S., 2004. The stability of tidal flats in Venice Lagoon — the results of in-situ measurements using two benthic, annular flumes. *Journal of Marine Systems.* (51), 211–241.

Barras J.A., Beville, S., and Britsch, D. 2003. Historical and projected coastal Louisiana land changes: 1978–2050. USGS. Open File Report 03–334.

Black, K.S., Tolhurst, T.J., Paterson, D.M., Hagerthey, S.E. 2002. Working with natural cohesive sediments. *Journal of Hydraulic Engineering-ASCE* 128 (1), 2–8.

Blum, M. D. and Roberts, H. H. 2012. The Mississippi Delta Region: Past, Present, and Future. *Annual Review of Earth and Planetary Sciences*, 40(1), 655–683.

Boesch, D. F., Josselyn, M. N., Mehta, A. J., Morris, J. T., Nuttle, W. K., Simenstad, C. A., and Swift, D. J. P. 1994. Scientific assessment of coastal wetland loss restoration and management in Louisiana. *Journal of Coastal Research Special Issue*, 20(103).

Brady, N.C., and Weil, R.R., 2002. The Nature and Properties of Soils. Prentice Hall, Upper Saddle River, N.J.. 960pp.

Brasher, M. G. *Review of the Benefits of Marsh Terraces in the Northern Gulf of Mexico*, Ducks Unlimited, Gulf Coast Joint Venture. 1-22.

Cangialosi, J., Hagen, A., and Berg, R. 2019. National Hurricane Center Tropical Cyclone Report – Hurricane Barry (AL022019). National Oceanic Atmospheric Administration Report.

Chabreck, R. H. 1970. Marsh zones and vegetative types in the Louisiana coastal marshes. Ph.D. thesis. Louisiana State University, Baton Rouge. p.113.

Coleman, J. M., and H. H. Roberts. 1989. Deltaic coastal wetlands: *Geologie en Mijnbouw*, (68), 1–24.

Correa, J., Postma, J. A., Watt, M., and Wojciechowski, T. 2019. Soil compaction and the architectural plasticity of root systems. *Journal of Experimental Botany*, *70*(21), 6019–6034. https://doi.org/10.1093/jxb/erz383

Couvillion, B.R., Barras, J.A., Steyer, G.D., Sleavin, William., Fischer, Michelle., Beck, Holly., Trahan, Nadine; Griffin, Brad., and Heckman, David, 2011. Land area change in coastal Louisiana from 1932 to 2010*: U.S. Geological Survey Scientific Investigations Map 3164*, scale 1:265,000, 12 p. pamphlet.

Costanza, R., Pe´rez-Maqueo, O., Martinez, M, L., Sutton, P., Anderson, S, J., and Mulder, K. 2008. The value of coastal wetlands for hurricane protection. *Ambio*, (37), 241–248.

Craig, N. J., Turner, R. E., and Day Jr. J. W. 1979. Land loss in coastal Louisiana. *Proceedings of the third coastal marsh and estuary management symposium.* Louisiana State University, Baton Rouge, Louisiana, USA. p.227-254.

CRMS (n.d.), Coastwide Reference Monitoring System, CRMS. Available from: https://lacoast.gov/crms/ (Accessed 29 January 2020)

Day, J. W., Katrina, R., Boesch, D. F., Clairain, E. J., Kemp, G. P., Laska, S. B., et al. (2007). Restoration of the Mississippi Delta: Lessons from Hurricanes Restoration of the Mississippi Delta: Lessons from Hurricanes Katrina and Rita. *Science*, *315*, 1679–1685. https://doi.org/10.1126/science.1137030

Dean, R.G., and Dalrymple, R.A. 1991. Water Wave Mechanics for Engineers and Scientists. *Advanced Series on Ocean Engineering*, (2). http://dx.doi.org/10.1142/1232

Fagherazzi, S., and Wiberg, P. L. 2009. Importance of wind conditions, fetch, and water levels on wave-generated shear stresses in shallow intertidal basins. *Journal of Geophysical Research: Earth Surface*, 114(3), 1–12. https://doi.org/10.1029/2008JF001139

Feng, Z., and Li, C., 2010. Cold-front-induced flushing of the Louisiana Bays. *Journal of Marine Systems*, (*82)*, 252–264.

Garrison, T., and R. Ellis (2018), *Essentials of oceanography*, National Geographic Learning, Australia.

Gebert, J., Kothe, H., and Grongroft, A., 2006. Prognosis of methane formation by river sediments. *Journal of Soils and Sediments* 6 (2), 75–83.

Gosselink, J. G., Coleman, J. M., and Stewart, Jr. R. E. 1998. Coastal Louisiana. Status and trends of the nation's biological resources U.S. Department of the Interior, U.S. Geological Survey, Reston, Virginia, USA. (1), 385-436.

Grabowski, R. C., Droppo, I. G., and Wharton, G. 2010. Estimation of critical shear stress from cohesive strength meterderived erosion thresholds. *Limnology and Oceanography: Methods*, (8), 678–685. https://doi.org/10.4319/lom.2010.8.678

Grabowski, R. C., Droppo, I. G., and Wharton, G. 2011. Erodibility of cohesive sediment: The importance of sediment properties. *Earth-Science Reviews*, 105(3–4), 101–120. https://doi.org/10.1016/j.earscirev.2011.01.008

Graf, G., and Rosenberg, R., 1997. Bioresuspension and biodeposition: a review. *Journal of Marine Systems* 11 (3–4), 269–278.

Grim, R., 1962. Applied Clay Mineralogy. McGraw-Hill, New York. 430pp.

Guo, B., Subrahmanyam, M. V, and Li, C. 2020. Waves on Louisiana Continental Shelf Influenced by Atmospheric Fronts, 1–9. https://doi.org/10.1038/s41598-019-55578-w

Harraz, H. Z. 2016. *Clay Mineralogy*

Henry, W. K. 1979. Some aspects of the fate of cold fronts in the Gulf of Mexico. *Monthly Weather Review.* (107), 1078–1082.

Holmes, C. W., Caplan Steigleder, J., and Tunnell, J. W. 2009. Mississippi River Delta Plain, Louisiana Coast, and Inner Shelf Holocene Geologic Framework, Processes, and Resources. *Gulf of Mexico: Origin, Waters, and Biota Volume III Geology*, 175–193.

Houwing, E.J., 1999. Determination of the critical erosion threshold of cohesive sediments on intertidal mudflats along the Dutch Wadden Sea Coast. *Estuarine Coastal and Shelf Science* 49(4), 545–555.

Hoyt, J.H., 1969, Chenier versus barrier, genetic and stratigraphic definition: American Association of Petroleum Geologists Bulletin, v. 53, p. 299–306.

Huang, W., & Li, C. (2019). Estuarine, Coastal and Shelf Science Spatial variation of cold front wind-driven circulation and quasi-steady state balance in Lake Pontchartrain Estuary. *Estuarine, Coastal and Shelf Science*, *224*(March), 154–170. https://doi.org/10.1016/j.ecss.2019.04.031

Jepsen, R., Roberts, J., and Lick, W., 1997. Effects of bulk density on sediment erosion rates. *Water Air and Soil Pollution* 99(1–4), 21–31.

Johnson, B.D., Kranck, K., and Muschenheim, D.K., 1994. Physicochemical Factors in Particle Aggregation. In: Wotton, R.S. (Ed.), The biology of particles in aquatic systems. Lewis, Boca Raton, pp. 75–96.

Kandiah, A., 1974. Fundamental aspects of surface erosion of cohesive soils. PhD Thesis, University of California, Davis.

Kolb, C.R., and Van Lopik, J.R., 1958, Geology of the Mississippi deltaic plain: U.S. Army Corps of Engineers, Waterways Experiment Station, Technical Report 2, 482 p.

La Peyre, M. K., Gossman, B., and Nyman, J. A. 2007. Assessing functional equivalency of nekton habitat in enhanced habitats: Comparison of terraced and unterraced marsh ponds. *Estuaries and Coasts*, *30*(3), 526–536.

Li, C., H. Roberts., Stone, G. W., Weeks, E., and Luo, Y. 2010. Wind surge and saltwater intrusion in Atchafalaya Bay during onshore winds prior to cold front passage, *Hydrobiologia*, 658(1), 27–39.

Lick, W., Jin, L.J., Gailani, J., 2004. Initiation of movement of quartz particles. *Journal of Hydraulic Engineering-ASCE*, 130 (8), 755–761.

Lick, W., McNeil, J., 2001. Effects ofsediment bulk properties on erosion rates. *Science of the Total Environment* 266 (1–3), 41–48.

Lindquist, D. C. 2008. *Ecological Review*, rep.

Lovelace, Jacob. B., and Smee, Delbert. Lee. 2018. Assessing the Efficacy of Marsh Restoration via Terracing by Comparing Vegetation Density and Nekton Abundance Before and After Restoration. *Gulf of Mexico Science*, 2018(1), 56–62.

Mehta A.J. 1988. Laboratory Studies on Cohesive Sediment Deposition and Erosion. In: Dronkers J., van Leussen W. (eds) *Physical Processes in Estuaries*. Springer, Berlin, Heidelberg.

Meysman, F.J.R., Middelburg, J.J., and Heip, C.H.R. 2006. Bioturbation: a fresh look at Darwin's last idea. *Trends in Ecology & Evolution* 21 (12), 688–695.

Mitchener, H., Torfs, H., 1996. Erosion of mud/sand mixtures. *Coastal Engineering* 29 (1–2), 1–25.

Moller, O. O., Lorenzzetti, J. A., Stech, J. L. and Mata, M. M. 1996. The summertime circulation and dynamics of Patos Lagoon. *Continental Shelf Research*. (16), 355-351.

Morgan, R.P.C., 2005. Soil Erosion and Conservation. Blackwell, Oxford. 304pp.

Morton, R. 2017. Subsidence and Wetland Loss Related to Fluid Energy Production, Gulf Coast Basin. Available from: https://archive.usgs.gov/archive/sites/coastal.er.usgs.gov/gc-subsidence/index.html (Accessed 2 February 2020).

Myrhaug, D. 2017. ScienceDirect Wave-induced bottom shear stress estimation in shallow water exemplified by using deep water wind statistics. *Oceanologia*, *59*(2), 102–107. https://doi.org/10.1016/j.oceano.2016.09.002

Nese, J. M. and Grenci, L. M. A 2006. World of weather: fundamentals of meteorology 780 Kendall/Hunt Publishing Co.

Nienhuis, J. H., Ashton, A. D., Nardin, W., Fagherazzi, S., and Giosan, L. 2016. What makes a delta wave-dominated? Earth Surface 664–683. https://doi.org/10.1002/2015JF003780

O'Connell, J. L., and Nyman, J. A. 2010. Marsh terraces in coastal Louisiana increase marsh edge and densities of Waterbirds. *Wetlands*, *30*(1), 125–135.

Osorio, R. J., Linhoss, A., and Dash, P. 2020. Evaluation of Marsh Terraces for Wetland Restoration: A Remote Sensing Approach. *Water*, 1–18. https://doi.org/10.3390/w12020336

Owen, D.E., 2008. Geology of the Chenier Plain of Cameron Parish, southwestern Louisiana, in Moore, G., ed.: Geological Society of America Field Guide 14, 2008 Joint Annual Meeting, Houston, Texas, 5–9 October 2008, p. 27–38, doi: 10.1130/2008.fl d014

Panagiotopoulos, I., Voulgaris, G., Collins, M.B., 1997. The influence of clay on the threshold of movement of fine sandy beds. *Coastal Engineering,* 32 (1), 19–43.

Partheniades, E., 2007. Engineering Properties and Hydraulic Behavior of Cohesive Sediments. CRC, Boca Raton. 338pp.

Penfound, W. T., and E. S. Hathaway. 1938. Plant communities in the marshlands of southeastern Louisiana. *Ecological Monographs* (8):1-56.

Peyronnin, N., Green, M., Richards, C. P., Owens, A., Reed, D., Chamberlain, J., Groves, G. G., Rhinehart, W. K., and Belhadjali, K. 2013. Louisiana's 2012 Coastal Master Plan: Overview of a Science-Based and Publicly Informed Decision-Making Process. *Journal of Coastal Research*, (69), 1–15.

Reed, D. J., and Wilson, L. 2004. "Coast 2050: A new approach to restoration of Louisiana coastal wetlands." *Physical Geography*, 25(1), 4-21.

Righetti, M., and Lucarelli, C., 2007. May the Shields theory be extended to cohesive and adhesive benthic sediments? *Journal of Geophysical Research-Oceans,* 112, C05039.

Roberts, H. H., DeLaune, R. D., White, J. R., Li, C., Sasser, C. E., Braud, D., Weeks, Edward., and Khalil, Syed. 2015. Floods and Cold Front Passages: Impacts on Coastal Marshes in a River Diversion Setting (Wax Lake Delta Area, Louisiana). *Journal of Coastal Research*, *315*(5), 1057–1068.

Roberts, J., Jepsen, R., Gotthard, D., and Lick, W., 1998. Effects of particle size and bulk density on erosion of quartz particles. *Journal of Hydraulic Engineering-ASCE*, 124 (12), 1261–1267.

Ravisangar, V., Sturm, T.W., and Amirtharajah, A., 2005. Influence of sediment structure on erosional strength and density of kaolinite sediment beds. *Journal of Hydraulic Engineering-ASCE,* 131 (5), 356–365.

Rowell, D.L., 1994. Soil Science: Methods and Applications. Longman, Harlow. 350pp.

Rozas, L. P., and Minello, T. J. 2001. Marsh terracing as a wetland restoration tool for creating fishery habitat. *Wetlands*, *21*(3), 327–341.

Ruckelshaus, M., Doney, S. C., Galindo, H. M., Barry, J. P., Chan, F., and Duffy, J. E. 2013. Securing ocean benefits for society in the face of climate change. *Marine Policy*, (40), 154–159. https://doi.org/10.1016/j.marpol.2013.01.009

Sgro, L., Mistri, M., and Widdows, J., 2005. Impact of the infaunal Manila clam, Ruditapes philippinarum, on sediment stability. *Hydrobiologia* (550), 175–182.

Sherwood, C. 2004. Wave-current model from Soulsby (1997) (MATLAB CODE).

Simon, A., Pollen, N., and Langendoen, E. 2006. Influence of two woody riparian species on critical conditions for streambank stability: Upper Truckee River, California. *Journal of the American Water Resources Association* 42 (1), 99–113

Smith, J. M. 1991. Wind Wave Generation On Restricted Fetches, US Army Corps of Engineers, Vicksburg, MS.

Smith, M., and Bentley, S. J. 2015. Sediment capture in flood plains of the Mississippi River: A case study in Cat Island National Wildlife Refuge, Louisiana. *Proceedings of the International Association of Hydrological Sciences*, *367*, 442–446. https://doi.org/10.5194/piahs-367-442-2015

Soulsby, R. 1997. *Dynamics of marine sands: a manual for practical applications*, Telford, London.

Steyer, G.D., Sasser, C.E., Visser, J.M., Swenson, E.M., Nyman, J.A., and Raynie, R.C. 2003. A proposed coast-wide reference monitoring system for evaluating wetland restoration trajectories in Louisiana: *Environmental Monitoring and Assessment*, (81) 107–117.

Sweet, W.V., R.E. Kopp, C.P. Weaver, J. Obeysekera, R.M. Horton, E.R. Thieler, and C. Zervas, 2017. *Global and Regional Sea Level Rise Scenarios for the United States*. NOAA Technical Report NOS CO-OPS 083. NOAA/NOS Center for Operational Oceanographic Products and Services.

Thayer, G.W., T.A. McTigue, R.J. Salz, D.H. Merkey, F.M. Burrows, and P.F. Gayaldo. 2005. *Science-Based Restoration Monitoring of Coastal Habitats, Volume Two: Tools for Monitoring Coastal Habitats. NOAA Coastal Ocean Program Decision Analysis Series 23:2*. Silver Spring, MD. 628p.

Trahan, A. 2017. Final Environmental Assessment Terracing and Marsh Creation South of Big Mar Bs-24 Environmental Assessment Terracing and Marsh Creation South of Big Mar. U.S. Fish and Wildlife Services. Report. 43p.

Trosclair, K. J. 1995. Wave transformation at a saltmarsh edge and resulting marsh edge erosion: observations and modeling. Master's Thesis. Baton Rouge, Louisiana. Louisiana State University. 73p.

Turner, R. E., Baustian, J. J., Swenson, E. M., and Spicer, J. S. 2006. Wetland Sedimentation from Hurricanes Katrina and Rita. *Science Express,* Report 449–453.

Turner, R. E., and B. Streever. 2002. Approaches to coastal wetland restoration: Northern Gulf of Mexico. SPB Academic Publishing, The Hague, Netherlands.

Underwood, G.J.C., Paterson, D.M., and Parkes, R.J., 1995. The measurement of microbial carbohydrate exopolymers from intertidal sediments. Limnology and Oceanography 40 (7), 1243–1253

USDA. 2001. Soil Survey Field and Laboratory Methods Manual. Soil Survey Investigations Report No. 51, Burt and Soil Survey Staff (ed.). U.S. Department of Agriculture, Natural Resources Conservation Service.

Walker, N.D. and Hammack, A.B., 2000. Impacts of winter storms on circulation and sediment transport. Atchafalaya-Vermillion Bay Region, Louisiana, U.S.A. *Journal of Coastal Research*, 16(4), 996– 1010.

Wiberg, P. L., and Sherwood, C. R. 2008. Calculating wave-generated bottom orbital velocities from surface-wave parameters. *Computers and Geosciences*, *34*(10), 1243–1262. https://doi.org/10.1016/j.cageo.2008.02.010

Wildish, D., and Kristmanson, D.D., 1997. Benthic Suspension Feeders and Flow. Cambridge University Press, Cambridge. 409pp.

Winterwerp, J.C., van Kesteren, W.G.M., 2004. *Introduction to the Physics of Cohesive Sediment in the Marine Environment.* Elsevier, Amsterdam. 576pp.

Wiseman W.J., Rabalais N.N., Turner R.E., Dinnel S.P., and MacNaughton A. 1997. A seasonal andinterannual variability within the Louisiana coastal current: stratification and hypoxia. Journal ofMarine Systems. (12), 237–248.

Whitehouse, R., Soulsby, R., Roberts, W., and Mitchener, H., 2000. *Dynamics of estuarine muds*, Telford, London.

Wotton, R.S., 2005. The essential role of exopolymers (EPS) in aquatic systems, oceanography and marine biology: an annual review. *Oceanography and Marine Biology* 57–94.

Yuill, B.; Lavoie, D.; and Reed, D. J., 2009. Understanding Subsidence Processes in Coastal Louisiana. *Journal of Coastal Research*, (54), 23–36.

APPENDIX A

SUPPLEMENTARY TABLES

Table A.1 Sediment sub-sample values from Miller property. Density calculated from 15 ml sample. τs calculated from Mehta 1988.

Platform				Terrace			
Sample #	Weight g	Density g/cm^3	τ cr N/m^2	Sample #	Weight g	Density g/cm^3	τ cr N/m^2
1.1	16.99	1.133	0.133	6.1	20.4	1.360	0.360
1.2	15.8	1.053	0.053	6.2	19.67	1.311	0.311
1.3	16.9	1.127	0.127	6.3	19.84	1.323	0.323
1.4	16.37	1.091	0.091	6.4	20.26	1.351	0.351
1.5	16.8	1.120	0.120	6.5	20.22	1.348	0.348
2.1	19.97	1.331	0.331	7.1	20.85	1.390	0.390
2.2	18.35	1.223	0.223	7.2	21.61	1.441	0.441
2.3	20.26	1.351	0.351	7.3	19.83	1.322	0.322
2.4	21.06	1.404	0.404	7.4	21.72	1.448	0.448
2.5	20.56	1.371	0.371	7.5	24.07	1.605	0.605
3.1	16.81	1.121	0.121	8.1	28.14	1.876	0.876
3.2	17.2	1.147	0.147	8.2	28.31	1.887	0.887
3.3	17	1.133	0.133	8.3	28.25	1.883	0.883
3.4	16.47	1.098	0.098	8.4	23.15	1.543	0.543
3.5	17.33	1.155	0.155	8.5	22.15	1.477	0.477
4.1	17.05	1.137	0.137	9.1	22.61	1.507	0.507
4.2	17.6	1.173	0.173	9.2	21.07	1.405	0.405
4.3	17.54	1.169	0.169	9.3	20.32	1.355	0.355
4.4	16.66	1.111	0.111	9.4	23.2	1.547	0.547
4.5	15.9	1.060	0.060	9.5	22.7	1.513	0.513
5.1	18.27	1.218	0.218	10.1	22.33	1.489	0.489
5.2	19.92	1.328	0.328	10.2	19.87	1.325	0.325
5.3	20.84	1.389	0.389	10.3	22.77	1.518	0.518
5.4	18.5	1.233	0.233	10.4	21.84	1.456	0.456
5.5	19.87	1.325	0.325	10.5	19.99	1.333	0.333

Table A.2 Sediment sub-sample values from Miami property. Density calculated from 15 ml sample. Ts calculated using Mehta 1988.

Platform				Terrace			
Sample #	Weight g	Density g/cm^3	τ_{cr} N/m^2	Sample #	Weight	Density	τ_{cr} N/m^2
10.1	18.55	1.237	0.237	1.1	21.80	1.453	0.453
10.2	18.31	1.221	0.221	1.2	20.40	1.360	0.360
10.3	18.01	1.201	0.201	1.3	21.40	1.427	0.427
10.4	17.11	1.141	0.141	1.4	20.50	1.367	0.367
10.5	18.12	1.208	0.208	1.5	20.76	1.384	0.384
7.1	18.18	1.212	0.212	2.1	21.44	1.429	0.429
7.2	18.17	1.211	0.211	2.2	23.50	1.567	0.567
7.3	18.16	1.211	0.211	2.3	21.99	1.466	0.466
7.4	18.35	1.223	0.223	2.4	22.04	1.469	0.469
7.5	18.04	1.203	0.203	2.5	23.01	1.534	0.534
6.1	17.91	1.194	0.194	3.1	24.36	1.624	0.624
6.2	18.40	1.227	0.227	3.2	22.55	1.503	0.503
6.3	16.49	1.099	0.099	3.3	23.14	1.543	0.543
6.4	17.46	1.164	0.164	3.4	21.98	1.465	0.465
6.5	16.10	1.073	0.073	3.5	22.22	1.481	0.481
8.1	18.23	1.215	0.215	4.1	20.62	1.375	0.375
8.2	18.74	1.249	0.249	4.2	21.55	1.437	0.437
8.3	18.70	1.247	0.247	4.3	22.75	1.517	0.517
8.4	18.80	1.253	0.253	4.4	21.98	1.465	0.465
8.5	18.40	1.227	0.227	4.5	23.08	1.539	0.539
11.1	17.11	1.141	0.141	5.1	21.75	1.450	0.450
11.2	16.30	1.087	0.087	5.2	21.08	1.405	0.405
11.3	16.80	1.120	0.120	5.3	20.45	1.363	0.363
11.4	16.10	1.073	0.073	5.4	21.05	1.403	0.403
11.5	18.40	1.227	0.227	5.5	21.55	1.437	0.437
				9.1	26.00	1.733	0.733
				9.2	28.20	1.880	0.880
				9.3	27.77	1.851	0.851
				9.4	28.02	1.868	0.868
				9.5	26.74	1.783	0.783

APPENDIX B

SUPPLEMENTARY FIGURES

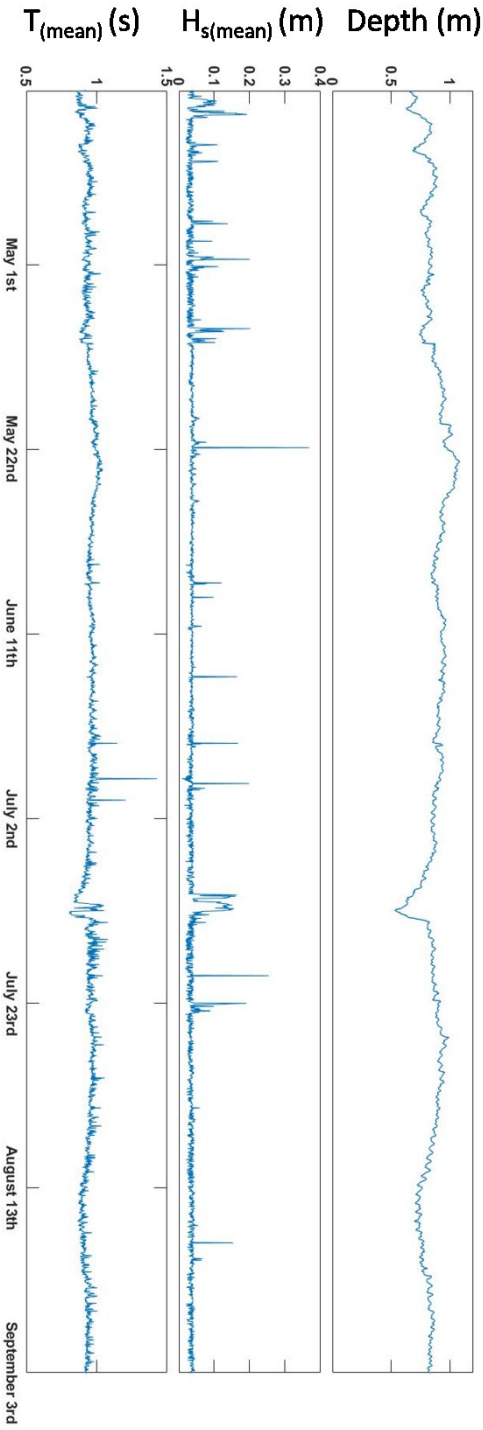

Figure B.1 Plots of water depth (m), significant wave height (m), and wave period (s) for the duration of the Miami deployment at ADCP 1.

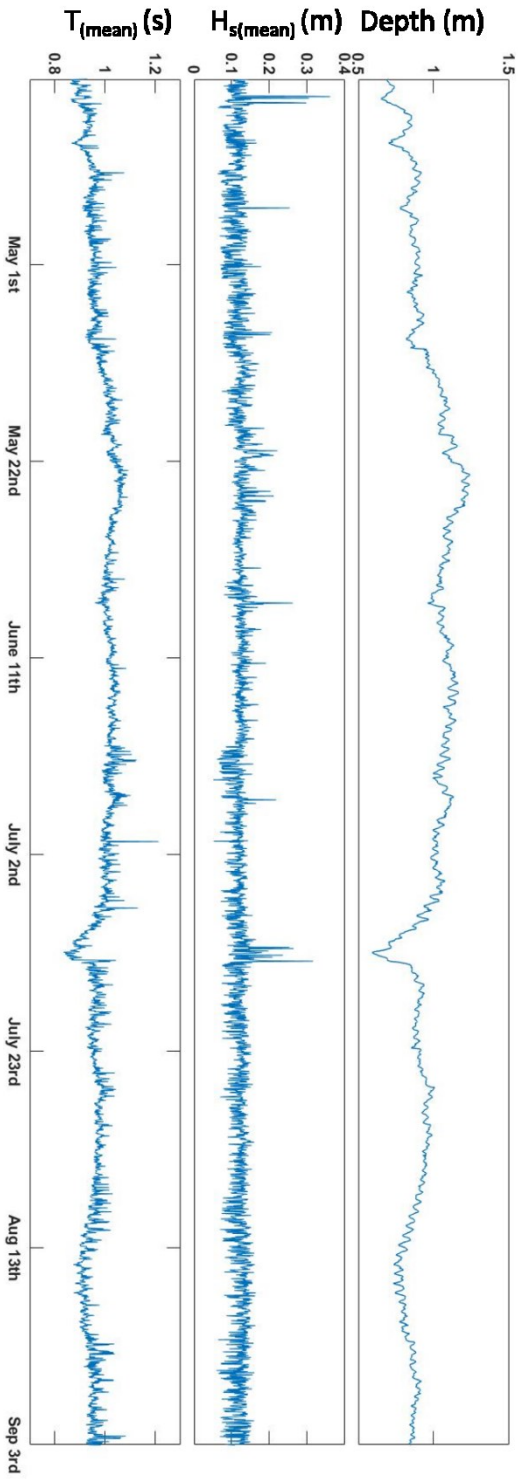

Figure B.2 Plots of water depth (m), significant wave height (m), and wave period (s) for the duration of the Miami deployment at ADCP 2

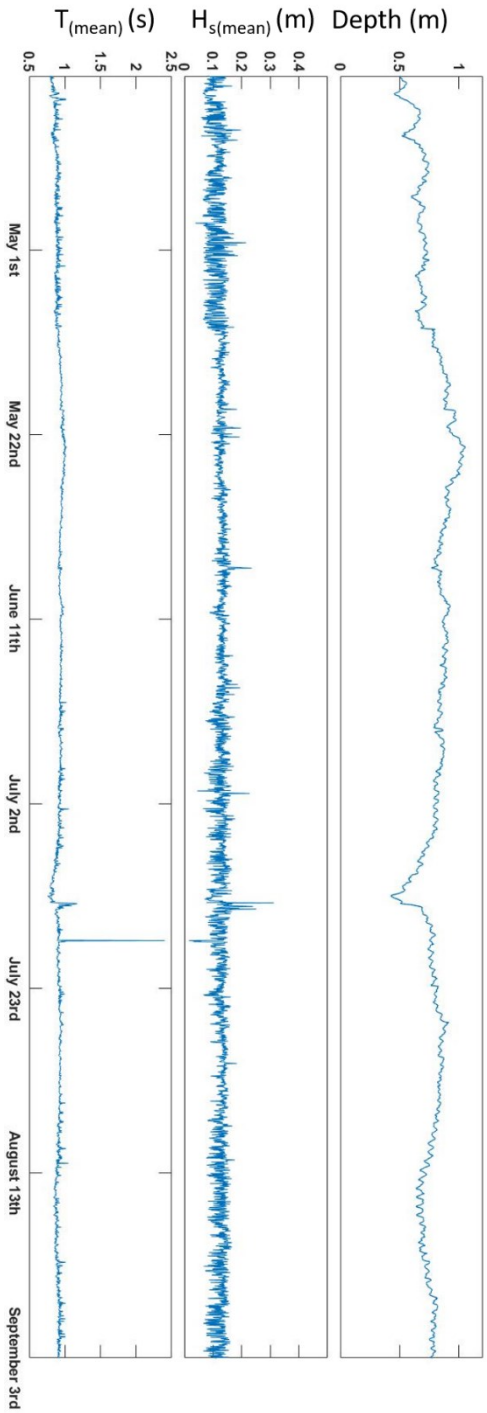

Figure B.3 Plots of water depth (m), significant wave height (m), and wave period (s) for the duration of the Miami deployment at ADCP 3

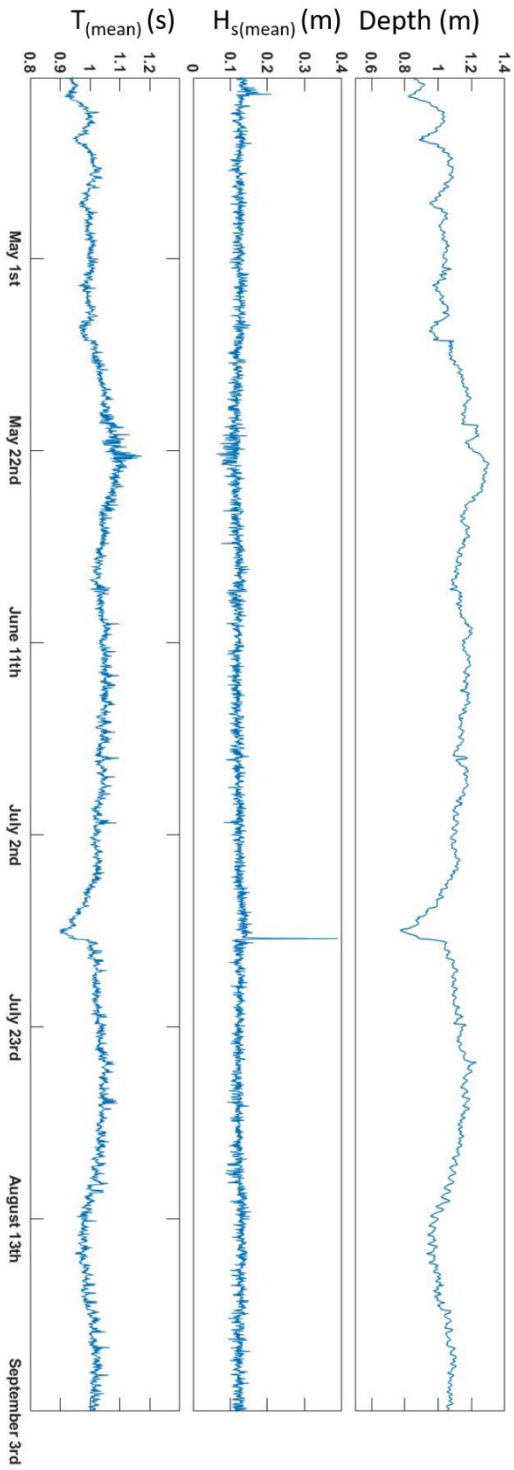

Figure B.4 Plots of water depth (m), significant wave height (m), and wave period (s) for the duration of the Miami deployment at ADCP 4

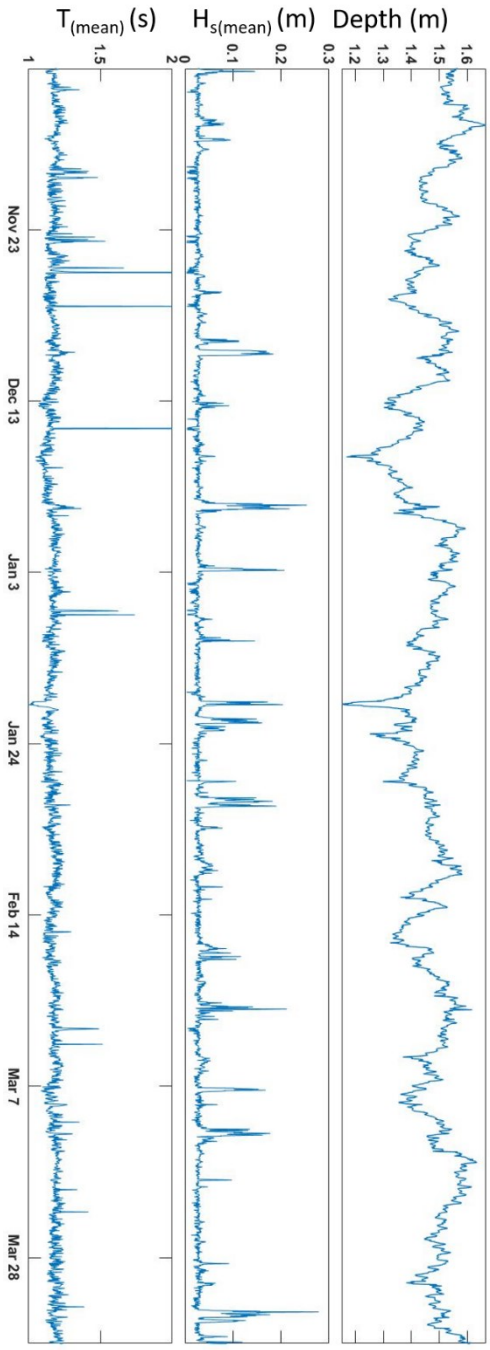

Figure B.5 Plots of water depth (m), significant wave height (m), and wave period (s) for the duration of the Miller deployment at ADCP 1

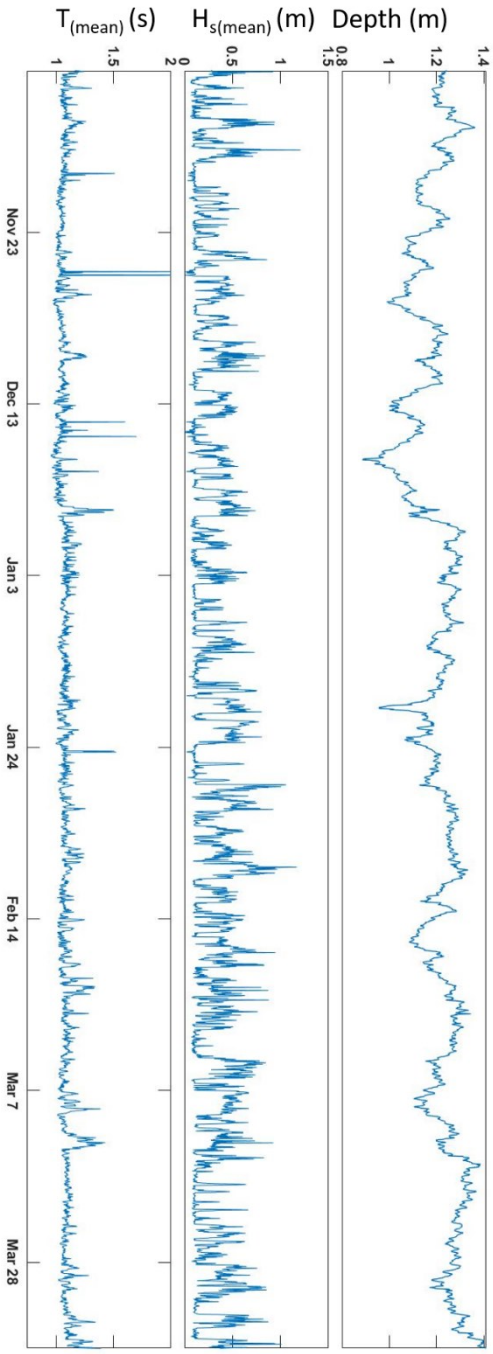

Figure B.6 Plots of water depth (m), significant wave height (m), and wave period (s) for the duration of the Miller deployment at ADCP 2

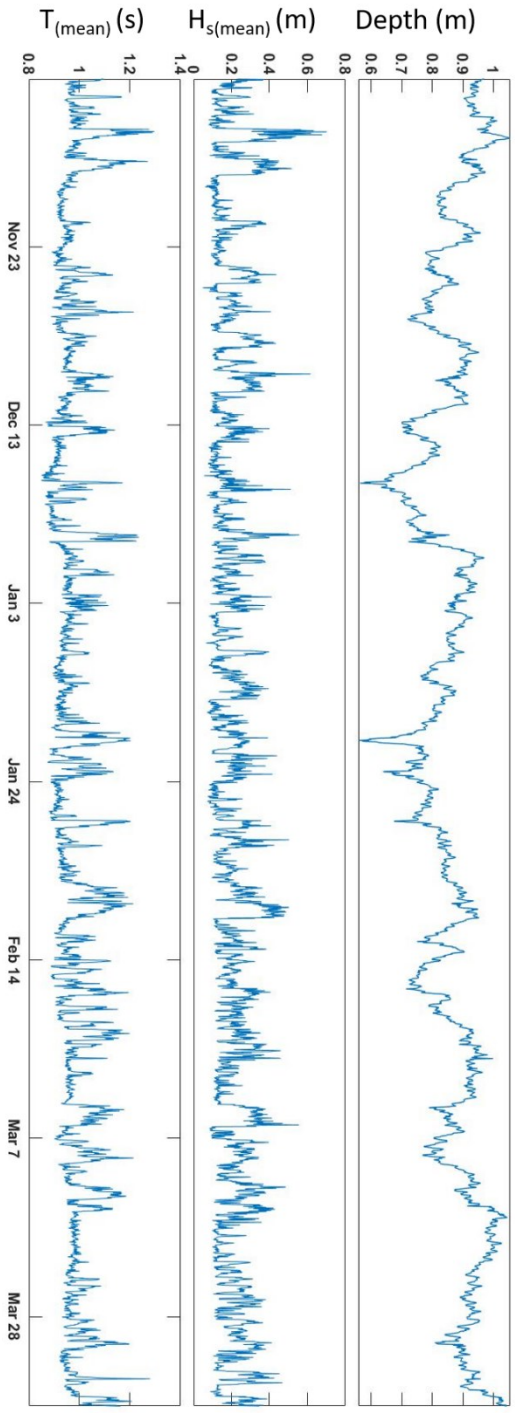

Figure B.7 Plots of water depth (m), significant wave height (m), and wave period (s) for the duration of the Miller deployment at ADCP 3

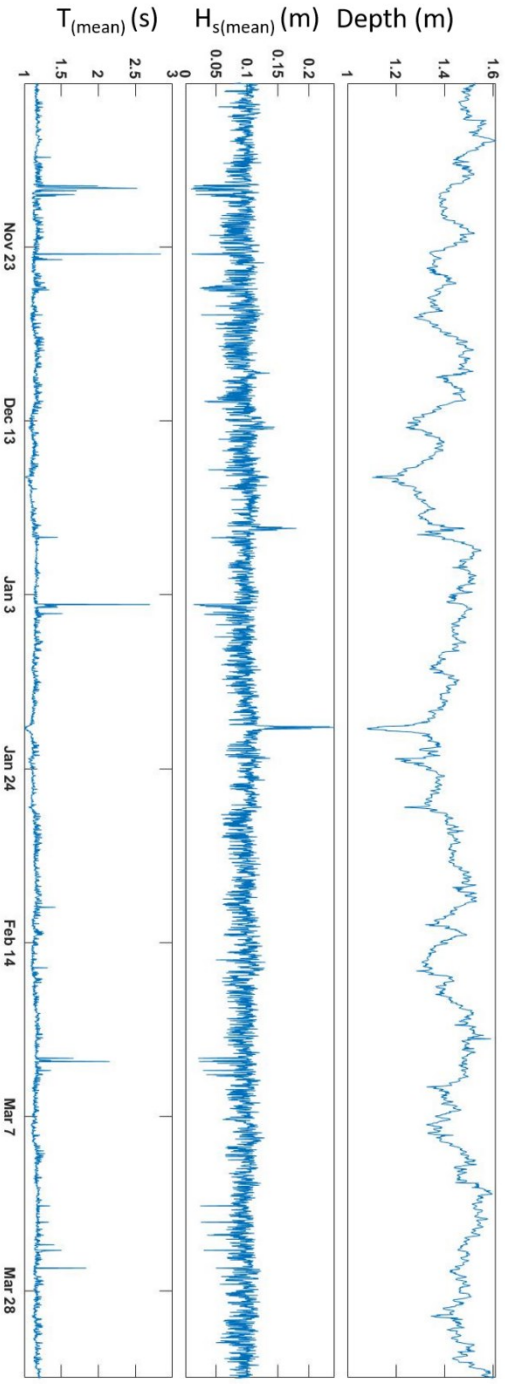

Figure B.8 Plots of water depth (m), significant wave height (m), and wave period (s) for the duration of the Miller deployment at ADCP 4